Range Anxiety

Panle Jia Barwick Shanjun Li Tianli Xia*

January 2026

Abstract

Range anxiety, the fear of depleting battery before reaching a charging station, is often cited as a major barrier to electric vehicle (EV) adoption, yet there has been limited formal economic analysis to quantify its magnitude and examine the policy implications. We develop a continuous-time dynamic model of EV usage and charging decisions to micro-found range anxiety as the utility loss from feasible yet unrealized trips due to perceived range constraints. Using high-frequency data of 188,000 EV trips and 26,000 charging events among 8,000 EVs in Shanghai, we recover model parameters governing consumer driving and charging decisions. The estimates imply that, across EV models with varying driving ranges, average range anxiety was about $1,900 in 2021 but declined to $1,200 in 2024, driven by improvements in charging infrastructure and, especially, increases in driving range. Policy simulations underscore the importance of coordinating investments in driving range and charging infrastructure to address range anxiety. Relative to socially optimal levels, Shanghai's EV market has under-invested in driving range but over-invested in charging infrastructure.

Keywords: Electric vehicles, range anxiety, charging infrastructure, dynamic model

JEL Classification Codes: L91, R13, R21

*Barwick: Department of Economics, UW-Madison, NBER, and CEPR, pbarwick@wisc.edu. Li: Doerr School of Sustainability and FSI, Stanford University, and NBER, shanli@stanford.edu. Xia: Simon Business School, University of Rochester, tianli.xia@rochester.edu. We thank Sarah Armitage, Jim Bushnell, Peter Christensen, Edward Glaeser, Yizhen Gu, Erich Muehlegger, Jing Li, Ming Li, Gabriel Kreindler, Emmanuel Saez, Jeremy West, Matthew Zaragoza-Watkins, and seminar and conference participants at Harvard, LSE, Rochester, UC-Davis, UC-Santa Cruz, and PKU-HSBC for their helpful comments. We thank Xiufang Cao and Yanhaohan Wen for excellent research assistance.

1 Introduction

With the transportation sector responsible for nearly one-third of global carbon emissions, transitioning to electric vehicles (EVs) powered by a clean energy grid has become a cornerstone of global decarbonization efforts. Since being introduced into the mass market in 2011, global passenger EV sales have grown rapidly, reaching 17.1 million units, or 20% of new passenger vehicle sales, by 2024.[1] Market penetration, however, varies widely: EVs accounted for 40% of new vehicle sales in China, 28% in Europe, 11% in the United States, and just 5% in the rest of the world. Even within countries or regions, adoption is highly uneven.[2] Understanding the barriers to EV adoption and identifying solutions to address them is critical for the next phase of EV diffusion.

Consumer surveys and industry reports regularly identify range anxiety as one of the most significant barriers to EV adoption (Wardlaw, 2020; Chokshi et al., 2021; Klier and Rubenstein, 2022; Rainieri et al., 2023; Bloomberg Intelligence, 2024). Range anxiety refers to the fear of depleting the battery before reaching a charging station, stemming from the combination of limited driving range and inadequate charging infrastructure.[3] Despite the widely recognized importance of range anxiety, formal analysis of the phenomenon and the cost-effectiveness of strategies to mitigate it remains limited. To bridge this gap, we develop a micro-foundation for range anxiety utilizing a continuous-time dynamic model of consumer EV usage and charging behavior. Based on estimated parameters, we quantify range anxiety in monetary terms and perform policy simulations to evaluate the relative efficiency of increasing vehicle driving range versus expanding charging infrastructure.

In the model, trip needs of varying distances arrive stochastically, and EV drivers decide whether to undertake a trip or initiate charging based on their remaining battery range, access to charging network, and charging prices. We define range anxiety as the utility loss from feasible but forgone trips, arising from the driver's perceived risk of battery depletion before reaching a charging station. Our empirical analysis leverages a unique, granular, and high-frequency dataset on EV driving and charging behavior. It records the location and remaining

[1] EVs include both battery electric vehicles (BEVs) and plug-in hybrid electric vehicles (PHEVs).

[2] Within Europe, EVs accounted for nearly 90% of new vehicle sales in Norway, compared to less than 20% in Germany. In the U.S., EVs made up about 26% of new car registrations in California in 2024, but less than 7% in Texas.

[3] Early EV models typically offered only 100–200 miles per charge, well below the 300–400 miles that gasoline vehicles can travel on a full tank. There were about 12,000 public EV charging stations in the U.S. in 2015. While the number grew to nearly 70,000 by 2025, it is still far fewer than the nearly 150,000 gasoline stations. In addition, EV charging infrastructure is found to be less reliable than gasoline stations, with one in every five EV chargers in the U.S. being out of order, reported by consumer reviews (Liu et al., 2023).

range of 8,000 EVs at 5-second intervals, along with detailed information on charging, such as station location, charging duration, price, and quantity. The data contains about 188,000 trips and 26,000 charging events across four weeks each in 2021 and 2024.

We begin by documenting some key patterns in the data. First, the charging probability, defined as the share of charging events among both driving and charging events, is higher when the remaining range (i.e., state of charge or SOC) is low. This is intuitive, as a limited remaining range both constrains the ability to take trips and increases the need to recharge. Second, the probability of charging rises with better charging access and falls with charging prices, the pattern becoming more pronounced at lower remaining ranges. Third, drivers with home charging access rely primarily on home charging to meet their needs. Their probability of using public fast charging is much less sensitive to remaining range than it is for those without home access, highlighting charging behavior differences between the two groups.

Empirical support for range anxiety stems from a robust pattern of "missing trips" in the data, defined as feasible trips that are foregone when they would result in a low SOC among BEVs. This pattern persists, though to varying degrees, across several sub-samples: daytime vs. nighttime, commuting time vs. leisure time, weekdays vs. weekends, winter vs. summer, and drivers with vs. without home chargers. However, a placebo test on PHEVs does not detect this pattern. To provide causalevidence, we conduct a regression analysis examining how the projected remaining range (after a trip) affects the hazard rate of trip-taking, and how this effect varies with charging density or access. To address potential endogeneity in charging access, we construct a shift-share instrument by interacting the pre-sample (2018) number of points of interest (POIs) with the declining cost of charging equipment over time. Our analysis shows that drivers forgo over 60% of trips that would reduce their remaining range below 50 km and approximately 14% of trips that would leave them between 50-100 km. Notably, improved charging access mitigates this behavior: the expansion of the charging network observed from 2021 to 2024 reduces the frequency of missing trips by nearly one-quarter.

Guided by these data patterns, we develop and estimate a continuous-time dynamic model to recover the structural parameters governing driving and charging decisions. We incorporate rich consumer heterogeneity and state variables. Consumers are characterized by the full driving range of their EV (e.g., 250km vs. 400km), the charging network structure (2021 vs. 2024), and whether they have access to a home charger. The set of state variables for a driver at any given point in time includes the remaining range of his vehicle, attributes of his current location (number of local charging stations, local charging price, number of local amenities,

home vs. away from home), and whether at daytime or nighttime. The estimates suggest that the probability of charging decreases with remaining range and charging prices, but increases with better charging access and rises for vehicles with longer driving ranges. In contrast, the probability of driving rises with remaining range but drops sharply if taking a trip reduces the remaining range below 50 or 100 km, or if the trip ends in areas with sparse or costly charging options. Finally, the estimated price elasticity of charging demand at fast public stations is -0.98 for drivers without home charging and -0.28 for those with home charging. The lower elasticity among drivers with home charging likely reflects their infrequent use of public stations.

Using the estimated parameters, we find that the willingness to pay (WTP) for improvements in driving range and charging access is substantial, especially among drivers without home charging. In 2018, the average driving range of the existing EV stock was 318km, and there wer only about 100 fast charging stations in the city. By 2024, the average range increased to 383km, while the number of fast charging stations surged to 2,268 (with a total of 40,000 fast chargers). For drivers without home chargers, the estimated WTP for these improvements is ¥62,000 (approximately $8,600), compared with ¥18,000 (or $2,500) for those with home chargers. The WTP exhibits diminishing returns for both driving range and charging access. Moreover, the two attributes are substitutes: the combined WTP from improving both is smaller than the sum of their individual effects.

We next quantify range anxiety by monetizing the utility loss from feasible but unrealized trips due to fear of getting stranded on the road. The average range anxiety across vehicles with different ranges was $2,550 in 2018, falling to $1,900 in 2021 and $1,200 in 2024. The averages mask significant heterogeneity across EVs with different driving range. The decline in range anxiety over time reflects both the expansion of the charging network and, especially, improvements in driving range. Overall, the reduction in range anxiety accounts for over 50% of WTP for improved driving range and charging access among drivers without home chargers, and roughly 15% among those with home charging.

We use simulations to evaluate two common strategies for alleviating range anxiety: expanding charging infrastructure vs. increasing driving range. The socially optimal level of each is determined by maximizing the aggregate welfare, defined as consumer surplus net of the social costs of improving range (via larger battery capacity) and charging access (through denser station networks). Our results reveal that the actual levels of charging access and driving range in Shanghai's EV market deviate substantially from the social optimum. Between 2018 and 2024, driving ranges consistently fell short of optimal levels. Charging infrastruc-

ture, in contrast, was insufficient in 2018 and 2021 but expanded so rapidly that by 2024 the number of stations was roughly double the social optimum. These results highlight the need to better coordinate investments in charging networks and battery capacity, especially since both are often supported by government policies such as subsidies.

Our paper contributes to four strands of literature. First, it extends the extensive work on consumer demand for EVs. Prior studies have primarily examined barriers to EV adoption—such as high upfront purchase costs, limited access to charging infrastructure, and the role of government policies in addressing these challenges (Springel, 2021a; Rapson and Muehlegger, 2023; Bushnell et al., 2025). A key finding in this literature is the importance of indirect network effects (the "chicken-and-egg" problem), whereby charging infrastructure investment and EV adoption reinforce each other through positive spillovers (Li et al., 2017; Li, 2023; Springel, 2021b; Jacqz and Johnston, 2024; Wang, 2024). While range anxiety is frequently invoked as the implicit mechanism linking charging access to EV adoption, it has remained largely without a formal definition in the literature. Qin and Scott (2025) examine how driving range interacts with fuel prices to influence EV demand as a proxy for range anxiety because the disutility of limited range is magnified when lower fuel prices increase the demand for travel. More recently, Kaps et al. (2025) illustrate the presence of range anxiety by demonstrating that while BEVs and gasoline vehicles exhibit similar total mileage, BEVs are significantly less likely to be used for long-distance trips (exceeding 150 km), a gap that narrows as charging network density increases. In contrast, our paper provides a micro-foundation for range anxiety through a continuous-time dynamic model, allowing us to quantify range anxiety in a utility maximization framework using high-frequency data on driving and charging behavior.

Second, our paper contributes to the emerging literature on EV charging. A central question in this literature is how charging behavior responds to prices across different settings, including home, workplace, and public stations. Field experiments document substantial variation in price elasticities across contexts (Garg et al., 2024; La Nauze et al., 2024; Bernard et al., 2025; Bailey et al., 2025).[4] Relying on highly disaggregated data, other studies infer EV usage from household electricity consumption in California (Burlig et al., 2021), estimate the time cost of fueling gasoline vehicles among drivers in Michigan and use this estimate to benchmark the cost of charging (Dorsey et al., 2025), and examine the impact of charging on the electricity grid in Germany (Heid et al., 2024). Our paper extends this literature by exam-

[4]For example, interventions on charging prices yield elasticity estimates of –0.4 for workplace charging at UCSD (Garg et al., 2024), –0.44 for home charging among Tesla owners in Australia (La Nauze et al., 2024), and –1.6 for home charging in Calgary (Bailey et al., 2025). A UK national intervention at public charging stations finds price elasticities of -2 to -2.9 (Bernard et al., 2025), with considerable heterogeneity.

ining how driving and charging respond to both charging prices and charging access, within a unified framework applied to highly granular observational data. Our structural estimates indicate a price elasticity of –1 for public charging. Notably, EV drivers with home charging exhibit a stronger response to price changes at home than to prices at public stations.

Third, our study contributes to the literature on policy design aimed at promoting EV adoption and infrastructure investment. We quantify the interaction between driving range and charging access through a micro-founded model of EV driving and charging decisions. Zhou and Li (2018) highlight the critical role of indirect network effects in EV diffusion and argue that government intervention may be necessary to coordinate consumer adoption and infrastructure development. Barwick et al. (2024) and Remmy (2025) examine automakers' incentives in supplying product attributes such as driving range, showing that market power and network effects can lead to socially suboptimal outcomes. Relatedly, Arkolakis et al. (2025) and Barwick et al. (2025a) develop models to characterize optimal charging networks that account for road network and driving patterns. Sunada and Xia (2025) shows the importance of coordinated investment on charger speed and density. Complementing these studies, our analysis demonstrates that the combination of limited driving range (supplied by automakers) and sparse charging access (provided by station investors) is the fundamental source of range anxiety, and that this interaction jointly determines the socially optimal levels of vehicle range and charging network size.

Finally, our paper contributes to the literature on public-private interactions. Li and Springel (2025) study the relationship between public and private charging stations in the U.S. Cabral et al. (2025) examines the substitutability and complementarity between public and private R&D. Our policy simulations underscore the importance of coordinating policy instruments such as subsidies that target different market participants, echoing the insight from Liu (2025) on the value of a coordinated policy mix in the EV sector.

The remainder of the paper proceeds as follows. Section 2 describes the data and discusses key data patterns. Section 3 presents the empirical model and estimation strategy. Section 4 discusses the estimation results. Section 5 conducts policy simulations. Section 6 concludes.

2 Data Description and Evidence

2.1 Data Description

Background and Data Sources Our analysis draws on data from Shanghai, a city with 24.9 million residents and 4.15 million households, spanning an area roughly the size of the

state of Delaware. By the end of 2024, Shanghai had 5.1 million registered passenger vehicles, including 1.51 million EV, the largest EV stock of any single city in the world. In 2024 alone, 278,000 new EVs were sold in Shanghai, accounting for 45% of all new passenger vehicle sales, slightly above the national average of 40%.[5] For comparison, the state of California in the U.S. has 39 million residents and 25 million passenger cars, of which 2.2 million are EVs. In 2024, 443,000 new EVs were sold in the state, accounting for 25% of new vehicle sales.

Our main dataset consists of eight weekly cross-sections of detailed EV usage and driving records, with four weeks drawn from 2021 and four from 2024. The four weeks fall in January, March, August, and October and capture seasonal variations across the year. Each cross-section contains data on 1,100 battery EVs, randomly sampled from the active residential-use EV fleet in Shanghai, with complete information on all trips and charging events during the week. Trip records are based on GPS tracking and include driving location and distance, while charging records provide the state of charge (SOC, i.e., remaining battery capacity measured in percentage from 0% to 100%), charging duration, and price.

We classify the continuous vehicle telematics data into three distinct event types: trips, charging events, and parking. A trip is defined as a non-charging movement segment, beginning with vehicle start and ending with shut-off. Consecutive segments separated by intervals of less than two minutes are aggregated into a single trip.

Charging events are classified as public or private. A public charging event is constructed by combining the charging session with the immediately preceding and subsequent trips, provided they occur within thirty minutes of the session's start or end.[6] Conversely, private charging (or home charging) refers to sessions at chargers in residential areas or workplaces. These are typically restricted-access, slow AC units that do not impose commercial markups. Parking is defined as any period where the vehicle is turned off and not classified as a trip or charging event.

Applying these definitions yields a final sample of approximately 188,000 trips and 26,000 charging events. There are 8,500 commercial fast charging sessions and 17,500 private slow-charging sessions. We exclude public slow-charging events, as they are rare and account for less than 5% of the total. Table A1 reports summary statistics of the sample.

[5]Battery electric vehicles (BEVs) made up 71% of the EV stock and 89% of all new EV sales in Shanghai in 2024. Plug-in hybrid (PHEVs) accounted for the rest.

[6]On average, drivers travel 2 km and spend ten minutes reaching a public charging station (including potential waiting and setup time). The thirty-minute threshold serves as a conservative upper bound to accommodate unobserved heterogeneity in traffic conditions, while excluding longer, unrelated commutes. The number of charging events is robust to varying this threshold between 15 and 45 minutes. Trips following a private charging session are treated as separate trips.

Our second dataset, obtained from the Shanghai Electric Technology Center, covers all commercial fast charging stations in Shanghai from 2020 to 2024, including each station's location, posted prices, and hourly usage. Merging this data with the trip-level records allows us to measure the density of nearby fast charging options and the price menu available at alternative stations for every trip in the primary dataset. Appendix Figure A1 plots the spatial distribution and frequency of charging events for fast and slow stations using the primary trips data. These patterns align well with the location and usage statistics from the secondary dataset on charging stations, corroborating the representativeness of the trip sample. Figure A2 illustrates the average charging prices at fast charging stations disaggregated by location and time of day, revealing substantial spatio-temporal heterogeneity.

Our third dataset, provided by the Shanghai Municipal Government, contains time-of-use (TOU) electricity pricing schedules for residential and commercial charging. Appendix Figure A3 illustrates the hourly price trajectories across seasons. While the peak-load windows remain largely consistent throughout the year, the pricing structure varies seasonally: summer and winter seasons feature four distinct pricing tiers, whereas spring and autumn utilize a three-tier system. Although these rates do not exhibit spatial variation, they are characterized by significant fluctuations both across seasons and within daily hourly cycles.

Development Over Time Shanghai witnessed a substantial expansion of its charging network. The total number of fast chargers surged from 780 in January 2020 to 34,020 in December 2024, about a 44-fold expansion, with roughly 15 chargers per station on average (Figure 1).[7] For comparison, as of December 2024, California, with a land area over 60 times that of Shanghai, had about 15,000 fast chargers, while the entire United States had around 50,000. The bottom panel of Figure 1 maps fast charging access across the city, measured by the log of inverse distance-squared weighted sum of charging stations (measured in kilometers). For example, A value of 2 corresponds to 7.4 charging stations within 1km or 1.8 charging stations within 0.5 km. In 2021, only the central districts with the highest population density had charging access above 2.0; by 2024, most urban areas exceeded this threshold. The average charging access weighted by trip frequency across the entire city was 2.08 in 2021 and 2.84 in

[7]The rapid expansion was driven by significant reductions in the capital costs of charging infrastructure, generous investment subsidies, parking mandates, and a sharp increase in EV stock. The average capital cost of fast charging equipment fell from about 500 ¥/kW per charger in 2018 to 130 ¥/kW in 2024 (Gao, 2023). The Shanghai municipal government provided subsidies covering 10–30% of total investment costs and required 10–15% of parking spaces in newly built garages to be equipped for EV charging. During this period, the EV stock in Shanghai rose from 240,000 to more than 1.5 million, further stimulating market entry of charging facilities. Stations are owned by electric utilities, EV manufacturers, and, most commonly, independent network operators.

2024.

The average driving range of the existing EV stock in the main sample increased from 281 km in winter 2021 (January) to 331 km in winter 2024, as newer models tend to offer longer ranges (Figure 2, Panel (a)).[8] Weekly usage also rose: the average number of trips per EV grew by 25%, from 20 in winter 2021 to 25 in winter 2024, while the corresponding weekly driving distance increased by 36%, from 335 km to 457 km (Figure 2, Panels (b)-(c)). Patterns are similar in the other seasons, with trip counts and driving distance increasing across the board from 2021 to 2024.

The expansion of the charging network also helps explain the sharp decline in reliance on slow charging (or home charging, as slow charging in commercial stations in our sample is rare). The share of drivers who exclusively used slow charging fell from 76.9% to 53.6% from 2021 to 2024 (a 30% drop), likely reflecting improved availability and reliability of fast-charging infrastructure. Consistent with this, the average weekly frequency of fast charging per driver more than doubled from 0.7 in winter 2021 to 1.5 in winter 2024 (Figure 2, Panel (e)). Moreover, the average state of charge (remaining battery level) at the start of fast charging sessions increased from 36% to 40%, suggesting that drivers are charging more proactively rather than waiting until the battery is close to depletion (Figure 2, Panel (g)).

Overall, the data reveal a clear shift toward more frequent use of EVs and longer driving distances, in concert with the improvements in vehicle driving range and the rapid expansion of fast charging infrastructure. Together, these developments reflect the growing maturity of Shanghai's EV ecosystem between 2021 and 2024.

2.2 Charging Patterns

Our rich data on driving and charging trips reveal several interesting patterns. First, Figure 3 provides clear evidence that charging behavior is strongly influenced by the remaining battery level. Charging events (blue bars) are most likely to occur when the state of charge (SOC) is between 30% and 50%, and decline as SOC increases.[9] In contrast, driving events (pink bars) are much more likely when SOC is high, with more than 80% of trips occurring when the battery level exceeds $> 50\%$. The green line represents the fraction of charging events among

[8] Driving range is the lowest during winter months due to cold-weather battery inefficiency and increased auxiliary power use, trailing other seasons by approximately 70 km.

[9] Although U.S. EV drivers are often advised to maintain battery levels between 20% and 80%, we observe no adherence to this guideline in our setting. The distributions of battery levels at the start and end of charging events are smooth, with no evidence of bunching at the 20% or 80% thresholds (see Appendix Figure A8).

all events. It falls steadily with SOC, from about 70% when the remaining battery is below 10% to less than 10% when the remaining battery exceeds 80% of full capacity. Appendix Figure A4 reports the results separately for drivers with and without home chargers.

Second, fast charging decisions are influenced by both convenience and price. To illustrate this, Figure 4(a) presents a binned scatterplot of the charging probability (the ratio of charging trips to total trips) against station density, defined as the number of stations within 1 km (ranging from 1 to 15). We stratify the sample by the initial State of Charge (SOC $< 40\%$ versus SOC $\geq 40\%$) and fit lines to highlight the relationship. Figure 4(b) repeats the analysis and plots charging probability against the price at the nearest station.

As shown in Figure 4, charging behavior varies significantly with station availability, particularly when battery levels are low (SOC$<$40%). The probability of initiating a charging trip rises sharply with the number of nearby stations at low SOC levels, consistent with the hypothesis that greater local availability reduces search and hassle costs. In contrast, this relationship is much flatter for trips with SOC $> 40\%$, when drivers are less constrained and can afford to delay charging or travel further. Analogous heterogeneity holds for prices: charging events are more likely when prices are low, with low-SOC drivers exhibiting a stronger response to price differences.

Lastly, Figure 5 shows that drivers with home charging exhibit distinct patterns from those without. Those with home chargers primarily charge at home and use public fast chargers occasionally (e.g., for long-distance trips). They are also more likely to initiate charging at higher remaining battery levels than drivers without home chargers, likely reflecting the convenience of at-home charging.

2.3 Evidence on Range Anxiety

Raw Data Patterns We first examine range anxiety using raw data patterns. Figure 6 shows the hourly hazard rate of trip initiation (y-axis) against the remaining range at the start of the trip (x-axis), where the hazard rate is the ratio of the observed count of events to total exposure time, or $\frac{1}{\text{Exposure time}}$ in our setting. We stratify the data into three trip-length categories: $<$ 50 km, 50–100 km, and 100–150 km. The figure reveals a significant decline in the hazard rate for all three categories when the remaining range is low. The rate stabilizes once the remaining range exceeds 250 km (and especially 300 km). For instance, the hourly hazard rate for short trips ($<$ 50 km) is approximately 0.12 when the remaining range exceeds 250 km (i.e., 0.12 trips per hour), but drops to nearly 0.05 when the range falls between 50 and 100 km. Similar patterns persist for other trip lengths. This sharp decline in trip initiation at

lower ranges is consistent with range anxiety: drivers appear to forgo trips that would deplete the battery significantly (even if not fully), likely due to the fear of being unable to reach a charging station when needed.[10]

One might be concerned that the drop in the hazard rate at low remaining ranges is driven by factors other than range anxiety, such as weather or traffic conditions. As a placebo test, we plot the hazard rate for PHEVs in Appendix Figure A5. Unlike the pronounced drop observed for EVs, PHEVs show no comparable decline. This is consistent with the notion that range anxiety is largely irrelevant for PHEVs, which can switch to gasoline power when the remaining battery is low.

Figure A6 extends the analysis to different subsamples: daytime hours between 8am and 10pm (Panel a), weekend (Panel b), winter (Panel c), summer (Panel d), 2021 (Panel e), and 2024 (Panel f). While baseline hazard rates vary across subsamples, the decline in trip initiation at low ranges is universal. As expected, the hazard rate is highest during morning hours, which also exhibit the largest decline. Interestingly, there are more missing trips at low ranges in 2021 than in 2024. This likely reflects the substantial expansion of the charging network, which has helped mitigate range anxiety over time.

To the extent that drivers charge in anticipation of the next day's travel (planned charging), current SOC levels may be endogenous. To investigate this channel, Figure A7 plots the average SOC on the preceding day against the next day's longest trip distance (Panel a) and total driving distance (Panel b). We find no clear relationship between prior SOC and the next day's longest trip, and only a very weak correlation with total distance. This suggests that the observed decline in trip initiation at low SOC is unlikely to be an artifact of planned charging (i.e., drivers avoiding low SOC states prior to known trips), as the correlation between SOC and trip distance the next day is very weak.

An additional concern is that the observed behavioral shifts might be driven by the "20–80" rule of thumb, a widely cited heuristic advising drivers to maintain the SOC between 20% and 80% to preserve battery longevity. If followed, this practice could confound our identification of range anxiety. To evaluate this possibility, Figure A8 plots SOC levels immediately preceding and following each trip and charging session. The distribution reveals no systematic bunching at these intermediate thresholds; instead, the only significant concentration occurs at 100% following a charge. These patterns provide no evidence that drivers actively manipulate

[10]Beyond limited driving range and charging infrastructure, range anxiety can also stem from uncertainty regarding the accuracy of the reported remaining range, which fluctuates with driving conditions. While charger reliability is a documented concern exacerbating range anxiety in the U.S., it has not been reported as a widespread issue in Shanghai.

battery levels to adhere to the "20–80" range, reinforcing the conclusion that the observed decline in trip frequency at low SOC is attributable to range constraints rather than battery-preservation heuristics.

Causal Evidence A key empirical challenge is to separate the range anxiety from the confounders that low trip demand may correlate with low SOC. To tackle this, we turn to a regression analysis that leverages the granularity of our data. A central empirical implication of range anxiety is that it should be mitigated by improved charging access: drivers living and traveling in areas with greater charger density should exhibit less anxiety at low battery levels, and thus forgo fewer trips. Conversely, if the observed decline in trips at low remaining ranges were driven by confounders, such as unobserved low demand that coincides with low remaining ranges, we would expect the relationship between trip frequency at low SOC and local charging access to be weak or nonexistent.

To test this hypothesis, we calculate the number of trips originating from each *jiedao* (a sub-district administrative unit in Shanghai comparable to a census tract) for a given trip type i (defined as a unique combination of initial remaining range and trip distance).[11] Our empirical strategy hinges on the interaction terms between indicators of low remaining range and measures of charging access. These interactions allow us to test whether the behavioral response to low range is attenuated in areas with better charging infrastructure. Specifically, we estimate the following Poisson model of trip counts:

$$\begin{aligned}\mathbb{E}[\, y_{ijt} \mid X_{ijt}\,] = \exp\Big(&\beta_1 \mathbb{1}\{\text{post-range}_{it} < 50\} + \beta_2 \mathbb{1}\{50 \le \text{post-range}_{it} < 100\} && (1)\\ &+ \gamma_1 \mathbb{1}\{\text{post-range}_{it} < 50\} \times \text{CA}_{jt} + \gamma_2 \mathbb{1}\{50 \le \text{post-range}_{it} < 100\} \times \text{CA}_{jt} && (2)\\ &+ \ln(\text{exposure time}_{ijt}) + \eta_{\text{s(i)t}} + \delta_{\text{j}}\Big), && (3)\end{aligned}$$

where the outcome variable y_{ijt} denotes the total count of trips of type i observed in jiedao j during period t (t = 2021 or 2024). The term $\ln(\text{exposure time})_{ijt}$ represents the log of the total standing time for trip type i at location j and time t. We include this as an offset variable (fixing its coefficient to 1) to scale the outcome by the duration of opportunity, thereby ensuring the model estimates event rates rather than raw counts.[12]

[11] We restrict the sample to trips shorter than 250 km to mitigate observations with zero counts, as trips longer than 250 km are rare. We define five distance bins (< 50 km, 50–100 km, etc.) and nine starting range bins (50–100 km, 100–150 km, ..., 450–500 km). After excluding infeasible combinations (where the trip distance exceeds the starting range), we have 35 distinct trip types. Our spatial unit is the jiedao, a sub-district administrative unit in Shanghai comparable to a census tract. There are 225 jiedaos in Shanghai.

[12] In Poisson regression, the correct way to adjust for differing exposure durations is to include ln(exposure)

Our key explanatory variables identify trips that risk battery depletion. The indicator $\mathbb{1}\{\text{post-range}_{ijt} < 50\}$ equals 1 if completing the trip would reduce the remaining battery range to below 50 km. Similarly, $\mathbb{1}\{50 \leq \text{post-range}_{ijt} < 100\}$ identifies trips resulting in a remaining range between 50 and 100 km. The coefficients β capture the extent of forgone trips at these low levels (indicative of range anxiety), while the interaction coefficients γ estimate whether improved charging access mitigates this decline. We control for trip distance-by-year fixed effects, $\eta_{s(i)t}$, and jiedao fixed effects, δ_j.

A key empirical challenge is the potential endogeneity of charging access, which may correlate with unobserved shocks to trip demand. For example, commercial development in an area might simultaneously generate more trips and encourage investment in charging infrastructure. To address this, we construct a shift-share instrument by interacting the 2018 number of Point of Interest (POIs) with the time-varying construction costs of charging stations.[13] The instrument relies on the observation that charging stations are disproportionately sited near POIs. Thus, reductions in construction costs are likely to induce larger increases in station deployment in areas with a higher initial density of POIs. The 2018 POI distribution (which predates our sample) captures baseline exposure, determining how cost shocks differentially propagate across locations.

Table 1 reports the regression results. We find strong evidence of range anxiety, corroborating the graphical analysis. Across specifications, trips that would result in a remaining range of less than 50 km exhibit roughly a 60% reduction in the hazard rate.[14] Trips ending with 50–100 km of remaining range show a more moderate but still notable reduction of 14%, indicating that range anxiety persists even at these intermediate levels.

Charging access meaningfully alleviates range anxiety. In the PPML IV control-function specification (Column 3), a one-standard-deviation increase in charging access, roughly the observed change from the 2021 to the 2024 level, offsets roughly 15 percentage points (approximately one-quarter) of the decline in trip frequency for trips leading to remaining range < 50km, and about 7 percentage point (roughly half) of the decline for trips ending with a range of 50–100 km. Comparing the baseline estimates in Columns 1-2 with the IV results in Column 3 reveals a clear downward bias in the estimated mitigation effect. Jiedaos that

on the right-hand side as an offset rather than dividing the dependent variable by duration of exposure.

[13] A Point of Interest, POI, is a geo-tagged location such as a shop, restaurant, office, park, or transit station. Excluding charging stations, our baseline data from Gaode (a major location-based service provider in China) contains 1.23 million POIs in Shanghai as of 2018.

[14] PPML coefficients are in log-points. The exact percentage change is calculated as $\%\Delta = e^{\beta} - 1$. For example, a coefficient of -0.90 implies a reduction 59% ($e^{-0.90} - 1 \approx -0.59$), while a coefficient of -0.15 implies a reduction of 14%.

exhibit stronger range anxiety (with lower baseline trip rates) tend to attract more charging station investment between 2021 and 2024, creating a negative correlation between charging access and trip hazard. Failing to correct for this endogeneity biases the coefficients toward zero, leading to an underestimate of the role of charging infrastructure.[15]

Taken together, the graphical and regression analyses offer compelling evidence of range anxiety, indicating that certain trips were avoided because they would have ended with a low remaining range. We next turn to the structural model, which characterizes the underlying decisions that give rise to these missing trips and quantifies the extent of range anxiety.

3 Empirical Model of EV Usage and Charging

This section provides a micro-foundation of range anxiety by developing a continuous-time discrete-choice dynamic model to characterize EV driving and charging decisions. Range anxiety is captured by the utility loss from drivers' decisions to forgo certain trips that would leave the post-trip (ending) range low. We then translate the utility loss into monetary terms using the util-dollar conversion implied in the model.[16]

A continuous-time dynamic model has two advantages over a discrete-time approach. First, trips and charging events occur in continuous time with irregular intervals between them. A continuous-time model allows us to directly exploit variation in these intervals and avoids discretizing time into coarse units (e.g., hours), thereby eliminating discretization bias. Second, when multiple charging or driving events occur within a short period, the continuous-time framework does not require imposing an arbitrary ordering of events, since the probability that two events occur at exactly the same instant is zero by construction.

3.1 Setup

A representative driver of type i (type defined below) operates a vehicle with a full battery range of $\bar{R}_i$. Trip opportunities arrive according to a Poisson process. Upon arrival, the driver decides whether to undertake the trip. Accepting a trip yields utility but alters the state of the driver. For example, taking a trip reduces the remaining battery and relocates the vehicle to an area with different charging accessibility and amenities.

[15] Appendix Table A2 replicates this jiedao-level analysis for different types of trips. We find consistent patterns across trips at different times (commuting, weekend, summer, winter), and the biggest range anxiety is for commuting trips.

[16] The util per dollar is derived from the effect of charging prices on charging probabilities, which is standard in discrete-choice models.

Similarly, charging opportunities arrive via a Poisson process, at which point the driver decides whether to charge based on the current state (e.g., prevailing price). Charging restores the battery to its full capacity.[17] Our model treats trips and charging events as independent activities, effectively ruling out mid-route charging. This is consistent with inner-city EV driving patterns, where long detours for mid-trip charging are rare.[18] Thus, we model every charging event as a destination in itself. The key model elements are summarized below.

Driver Types We categorize drivers into I homogeneous types. Each type i is defined by a triplet comprising: 1) the vehicle's full battery range ($\bar{R}$), which bounds the maximum driving distance on a single charge; 2) the sample period (2021 vs. 2024), which captures temporal shifts in aggregate public charging infrastructure; and 3) home charger access (H), which reflects differences in charging costs.

The value function is solved independently for each driver type. While all driver types share a common set of state variables (that are described below), we specify type-specific transition processes to accommodate heterogeneous trip arrivals and charging availabilities. This is critical given the rapid evolution of EV technology and infrastructure between 2021 and 2024. By endowing each type with its own transition dynamics and value functions, the model flexibly captures how these technological and infrastructure improvements differentially impact driver utility.[19]

State Variables The driver's state is defined by six variables: remaining battery range, four location-specific attributes, and a time-of-day indicator (daytime vs. evening). The first state variable is the remaining battery range, $r \in \{0, 1, \ldots, 9\}$, which corresponds to ten 50-km bins (0-50 km, 50-100 km, ..., 450-500 km). The second variable, charging density (d), measures the convenience of the current location. We first calculate a continous measure of charging access, CA_l, defined as the inverse–squared-distance weighted count of stations within a 3 km radius: $CA_l = \sum_{k, \text{dist}^c_{lk} \leq 3km} \frac{1}{(\text{dist}^c_{lk})^2}$, where dist^c_{lk} is the distance between location l and

[17] In our sample, 82% of charging events restore the battery to full capacity (defined as [90%, 100%] of the total battery capacity). In a more general setting, a charging event could change the battery level to $r' > r$ with probability $p(r')$.

[18] We compared the travel time of observed charging trips against a hypothetical direct route from the pre-charging to post-charging location. In 90% of cases, the direct route is significantly shorter (by at least 50%), implying that charging is typically a primary destination rather than a detour on the way to another location.

[19] Alternatively, the three driver-type attributes could be incorporated directly into the state vector, expanding the state space to nine dimensions. Our approach allows us to solve the value function for each type in parallel and significantly reduces computational time.

station k.[20] Higher values of CA indicate greater local charging availability. We then create a categorical variable $d \in \{1, 2, 3, 4\}$ by grouping $\log(CA)$ into four bins based on the 2021 quartile cutoffs.

The third state variable captures access to amenities, specifically food and shopping locations. We define a continuous measure of amenity access, AA_l, for location l using a formulation analogous to that of charging access: $AA_l = \sum_{k, \text{dist}^a_{lk} \leq 3km} \frac{1}{(\text{dist}^a_{lk})^2})$, where dist^a_{lk} is the distance between location l and food/shopping store k. We then construct a categorical variable $a \in \{1, 2, 3, 4\}$ by binning $\log(AA)$ according to 2021 quartile cutoffs. Locations with greater amenity access are likely to be more desirable, as they offer greater trip utility and reduce opportunity costs of charging by allowing drivers to combine charging sessions with shopping or dining.

The fourth state variable is the charging price: $p = \{1, 1.3, 1.5, 2\}$ ¥/kWh, corresponding to the four most frequently observed tiers. The fifth state variable is only relevant to drivers with private charging: $h = \{0, 1\}$, which takes the value of 1 if the location is at a residential building or workplace. The sixth variable is a time-of-day indicator, $k = \{0, 1\}$, where $k = 1$ denotes daytime hours (08:00–20:00). Altogether, there are a total of 2,560 ($10 \times 4 \times 4 \times 4 \times 2 \times 2$) different state values.

Exogenous State Transitions The transition probability from state s to state s' is governed by the frequency of trips that move a driver between these states. We first describe the exogenous transition process generated solely by trip arrivals, and then turn to the endogenous transition process (i.e., the hazard rate), which combines exogenous trip arrivals with drivers' decisions to accept or decline a trip.

We use the matrix Λ_r to denote the transition probabilities of the remaining battery range. The $(r, r-j)$th entry corresponds to the probability that the battery range moves from level r to level $r - j$ as a result of taking a trip with length j ($j = 0, 1, \ldots, 9$, corresponding to the same set of bins as r: 0-50 km, 50-100 km, ..., 450-500 km). As shown in Figure 6, the trip hazard rate is roughly constant when the remaining range is over 300km. Our graphical and regression analysis suggests that the drop in trip frequency at the low remaining range was driven by range anxiety, rather than a decrease in the trip opportunities. Therefore, we assume that the arrival rate of trip opportunities with varying length j is independent of the remaining range. In other words, a trip of length 0-50 km arrives at the same rate regardless of whether the vehicle's remaining driving range is 200 km or 400 km. Consequently, we assume

[20] The 3km radius is roughly 10 minutes of city driving. The correlation between CA calculated using a 3km vs a 5km radius is nearly 1.0. Hence, the 3km threshold provides a good approximation of overall access.

that the transition matrix Λ_r has a Toeplitz structure: it is a lower-triangular matrix with constant values along each subdiagonal. Specifically,

$$\Lambda_r = \begin{bmatrix} \lambda_0 & 0 & 0 & \cdots & 0 \\ \lambda_1 & \lambda_0 & 0 & \cdots & 0 \\ \lambda_2 & \lambda_1 & \lambda_0 & \cdots & 0 \\ \vdots & \vdots & \vdots & \ddots & 0 \\ \lambda_9 & \lambda_8 & \lambda_7 & \cdots & \lambda_0 \end{bmatrix},$$

where λ_j denotes the arrival rate of a trip with length j.[21] All entries above the main diagonals are zero, since the battery level cannot increase without charging.

To account for temporal variations in trip arrival rates between daytime (8:00 AM – 8:00 PM) and evening (8:00 PM – 8:00 AM), we expand the arrival process using a transition-weighted matrix structure:

$$\Lambda_{rk} = \begin{bmatrix} \lambda_{k=0\to k=0}\Lambda_r(k=0), & \lambda_{k=0\to k=1}\Lambda_r(k=0) \\ \lambda_{k=1\to k=0}\Lambda_r(k=1), & \lambda_{k=1\to k=1}\Lambda_r(k=1) \end{bmatrix}.$$

In this formulation, $k \in \{0, 1\}$ represents the time period, where $k = 1$ denotes daytime and $k = 0$ denotes evening. The term $\Lambda_r(k)$ represents the trip frequency for period k. The scalar $\lambda_{k\to k'}$ represents the probability that a trip beginning in period k concludes in period k'.

It is important to note that the transition matrix Λ_{rk} remains stochastic even when trip patterns are deterministic or distances are fixed. For instance, consider a routine work commute. Despite the fixed destination, the remaining battery range upon arrival is inherently random, as energy consumption is influenced by exogenous factors such as traffic congestion, weather temperature (cold vs. hot days), and road topography. These variables can deplete battery capacity at rates significantly different from nominal conditions. Consequently, our derivation of Λ_{rk} relies on state-of-charge (SOC) rather than odometer readings, as the primary objective is to capture the stochastic evolution of available range over time. In robustness analyses, we allow Λ_{rk} to differ across driver types.

Let Λ_d denote the transition matrix of charging access. Each element $\lambda_{dd'}$ represents the probability that a trip takes the driver from a location with charging density (d) to one with density (d'). Since charging density has four levels, Λ_d is a 4×4 matrix. Similarly, Λ_a denotes the transition matrix for amenity access and Λ_p the transition probability of charging prices.

[21] The r^{th} row of Λ_r is set to zero if driver type i's vehicle has a full driving range shorter than r.

Both Λ_a and Λ_p are also 4×4 matrices. Finally, the probability that a trip returns the driver to their home charging location is given by a scalar, λ_h.

Assuming the (exogenous) transition process of different state variables is independent, the full transition matrix of moving from state s to state s', $\mathbf{q} \equiv \{q_{s,s'}\}$, is given by:

$$\mathbf{q} \equiv \Lambda_{rk} \bigotimes \Lambda_d \bigotimes \Lambda_a \bigotimes \Lambda_p \bigotimes \lambda_h, \tag{4}$$

where $\bigotimes$ is a Kronecker product.

Trip Utility Once a trip arrives, the deterministic part of the utility from taking the trip that moves from state s to state s' is given by:

$$\psi(1, s, s') = \alpha_0 + \alpha_1(r_s - r_{s'}) + \alpha_2 \mathbb{1}(r_{s'} = 2) + \alpha_3 \mathbb{1}(r_{s'} = 1), \tag{5}$$

where $r_{s'} = 2$ indicates that the remaining range after the trip is in the second bin, i.e., between [50km, 100km], and $r_{s'} = 1$ denotes the remaining range after the trip is in the first bin of [0km, 50km]. Parameter α_0 represents the baseline utility of a trip and α_1 is the premium for trips with a longer distance. α_2 and α_3, the key parameters of interest, capture the disutility associated with completing a trip at a low battery level, less than 50km or 100km, respectively. These two parameters are used to rationalize the missing trips, i.e., feasible but unrealized trips as shown in Figure 6. We use these parameters to quantifying range anxiety. Total utility also includes an idiosyncratic shock: $\tilde{\psi}(1, s, s') = \psi(1, s, s') + \varepsilon_{t,1}$ (where the subscript t denotes 'trip'). The utility of skipping the trip is normalized to zero plus a random shock: $\tilde{\psi}(0, s, s) = \varepsilon_{t,0}$. Without loss of generality, both shocks $\varepsilon_{t,1}$ and $\varepsilon_{t,0}$ are assumed to have variance 1.

We assume drivers always take the trip if the remaining battery level is above 300 km, corresponding to a cutoff $\bar{r} = 6$. In other words, we assume that range anxiety is irrelevant when the remaining battery is sufficiently high. If the remaining battery level is below 300 km, the driver decides whether to take the trip based on the trip utility. If the utility shock ε_t has a type I extreme-value distribution, the policy of taking the trip is given by:

$$\pi_{\text{trip}}(s, s') = \begin{cases} 1, & \text{if } r > \bar{r} \\ \frac{\exp[(\psi(1,s,s')+V(s')]}{\exp[\psi(1,s,s')+V(s')]+\exp[V(s)]}, & \text{if } r \leq \bar{r}, \end{cases} \tag{6}$$

where $V(s)$ and $V(s')$ are value functions defined in Section 3.2 below.

Incorporating both the exogenous transition process and the endogenous travel probability, the realized state transition process (i.e., hazard rate) is given by:

$$\tilde{\mathbf{q}} = \mathbf{q} \odot \mathbf{\Pi}_{\text{trip}}, \tag{7}$$

where $\odot$ denotes a Hadamard product, or an element-by-element product.

Charging Arrivals and Decisions The arrival rate of charging opportunities is denoted by λ_c. We assume four charging opportunities occur daily, $\lambda_c = 4$, roughly the same number of trips per day.[22] Upon the arrival of an opportunity, the driver decides whether to charge. Charging incurs a cost and fully replenishes the battery (with probability 1); all other state variables remain unchanged. Forgoing the opportunity keeps the state the same $s' = s$. We parameterize the deterministic component of charging costs as:

$$c(1, s) = \beta_0 + \beta_1 d_s + \beta_2 p_s, \tag{8}$$

where d_s is the charging density at state s and p_s is the charging price. More charging stations nearby reduce search and hassle costs. We estimate separate charging cost parameters for drivers without home chargers, those with home (private) chargers using public stations, and those charging at home. As with trip utility, total charging cost includes an idiosyncratic shock: $\tilde{c}(1, s) = c(1, s) + \varepsilon_{c,1}$. The cost of not charging is normalized to zero plus a random shock: $\tilde{c}(0, s) = \varepsilon_{c,0}$.[23]

Let $\bar{s} \equiv (r' = \bar{r}_i,\ d,\ p,\ h,\ k,\ a)$ denote the state immediately following a full charge, where $\bar{r}_i$ represents the range bin corresponding to the full battery capacity of driver i's vehicle. Assuming the cost shock ε_c is distributed type-I extreme value, the probability of charging conditional on an opportunity arising is given by:

$$\pi_{\text{chg}}(s) = \frac{\exp\big(c(1, s) + V(\bar{s})\big)}{\exp\big(c(1, s) + V(\bar{s})\big) + \exp\big(V(s)\big)}. \tag{9}$$

Combining the exogenous arrival rate of charging opportunities with the endogenous charging decisions, the hazard (realized) rate of charging is given by: $\tilde{\mathbf{q}}_{\text{chg}} = \lambda_c \mathbf{\Pi}_{\text{chg}}$.

[22] The total number of charging opportunities is analogous to the market-size measure in demand analyses. Results are robust to assuming $\lambda_c = 5$.

[23] The random shock $\varepsilon_{c,1}$ captures factors known to the driver but unobserved by the researcher, such as specific time constraints or anticipated future travel. Provided these unobserved factors are orthogonal to charging cost shifters, our framework yields consistent estimates of β.

Other Modeling Elements We assume flow utility $u(s) = 0$. That is, utility only comes from trips. We set the continuous-time discount rate at 0.1 per year, or a daily discount rate of $\rho = 0.999726$.

3.2 Bellman Equation

The Bellman equation characterizes the value function $V(s)$ in a continuous-time decision process where transitions occur stochastically. To gain intuition, consider a short time window Δt. The driver accrues an immediate flow utility $u(s)\Delta t$, which is assumed 0 in our setting. With probability $q_{ss'}\Delta t$, a trip opportunity arises that changes the state from s to s'. If the driver takes the trip, he gains trip utility $\psi(1, s, s')$. The continuation value changes to $V(s')$. Additionally, charging events occur with arrival rate $\lambda_c\Delta t$, and the driver decides whether to charge the vehicle to maximize the continuation value net of charging costs.

The probability that no events (neither a trip arrival nor a charging opportunity) occur within the time interval Δt is given by $1 - (\sum_{s'} q_{ss'} + \lambda_c)\Delta t$. With discounting, the resulting Bellman equation is:

$$\begin{aligned} V(s) = u(s) \times \Delta t + \sum_{s'} \frac{q_{ss'}\Delta t}{1+\rho\Delta t} E \max_{j\in\{0,1\}} \left\{ \underbrace{\psi(j=1,s,s') + V(s') + \varepsilon_{t,1}}_{\text{travel}}, \underbrace{V(s) + \varepsilon_{t,0}}_{\text{not travel}} \right\} \\ + \frac{\lambda_c \Delta t}{1+\rho\Delta t} E \max_{j\in\{0,1\}} \left\{ \underbrace{c(j=1,s) + V(\bar{s}) + \varepsilon_{c,1}}_{\text{charging}}, \underbrace{V(s) + \varepsilon_{c,0}}_{\text{not charging}} \right\} \\ + \frac{1 - \sum_{s'} q_{ss'}\Delta t - \lambda_c \Delta t}{1+\rho\Delta t} V(s). \end{aligned}$$

This equation approximates a continuous-time Hamilton-Jacobi-Bellman (HJB) equation as $\Delta t \to 0$. Solving the equation for $V(s)$ yields:[24]

$$\begin{aligned} V(s) = & \frac{\sum_{s'} q_{ss'} \left\{ \log \left[\exp[\psi(1,s,s') + V(s')] + \exp[V(s)] \right] + \gamma \right\}}{\lambda_c + \rho + \sum_{s'} q_{ss'}} \\ & + \frac{\lambda_c \log \left[\exp[c(1,s) + V(\bar{s})] + \exp[V(s)] \right] + \lambda_c \gamma}{\lambda_c + \rho + \sum_{s'} q_{ss'}} \end{aligned} \tag{10}$$

[24] Appendix Section A contains details about the derivation.

3.3 Estimation Details

We follow a two-step estimation procedure. In the first step, we recover the exogenous state arrival and transition process based on the observed trip arrivals and the time interval between these events. In the second step, we evaluate the empirical likelihood of observed trips and charging events and estimate structural parameters in trip utility and charging costs. This estimation procedure is similar to the discrete-choice dynamic model, but it leverages the time intervals between events in a continuous manner (via the hazard rates) and avoids the need to specify an arbitrary event ordering.

Estimating Exogenous Arrival Rates and Transition Probabilities Let $q_{s,s'}$ denote the transition probability from state s to s' as defined in Equation 4. The state vector s consists of six elements: the current battery level, local charging density, charging price, home (private) charging availability, local amenities, and a daytime indicator.

A primary empirical challenge is that observed trip frequencies at low battery levels likely underestimate the latent trip arrival rate, as drivers may strategically forgo travel to avoid the risk of battery depletion. To identify the underlying trip arrival parameters (Λ), we impose a behavioral assumption: range anxiety is not an issue when battery reserves are abundant. Specifically, for the subsample where the remaining range exceeds 300 km, we assume drivers accept all arriving trip opportunities. This identification strategy allows us to recover the latent trip arrival process from observed behavior in the high-range subsample.[25]

The probability that the state changes due to a trip arrival within τ units of time is:

$$1 - \exp\left[-\tau\left(\sum_{s'} q_{s,s'}\right)\right],$$

and the probability that the state does not change within τ units of time is defined analogously. This is the cumulative distribution function (cdf) of an exponential distribution with a transition rate equal to the aggregate trip frequency from state s to all reachable states s'. Differentiating this CDF with respect to the inter-arrival time τ yields the density function with the same rate parameter:

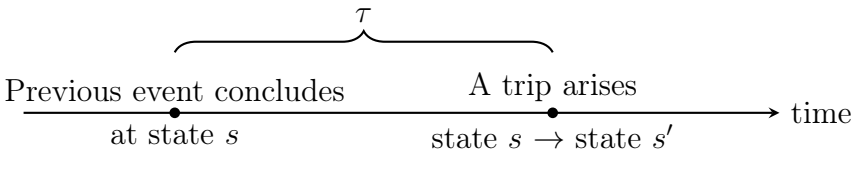
$$\left(\sum_{s'} q_{s,s'}\right) \exp\left[-\tau\left(\sum_{s'} q_{s,s'}\right)\right]. \tag{11}$$

[25] Should range anxiety persist even at high battery levels, our estimates would constitute a conservative lower bound on the true magnitude of the range anxiety effect.

Define $g(\tau, s; \mathbf{q}) = \exp\left[-\tau\left(\sum_{s'} q_{s,s'}\right)\right]$.

To construct the likelihood function for trip arrivals, we categorize the observed durations into two distinct types of intervals. In the first case, a trip arrives at time τ following the previous event, triggering a state transition from s to s' as illustrated below:

Case 1:

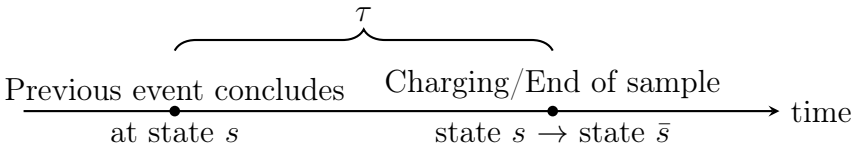


The corresponding likelihood is the product of a) the density function of a trip occurring at duration τ, and b) the probability of transitioning to state s' among all potential states:

$$L(\tau, s, s') = \underbrace{\left(\sum_{s'} q_{s,s'}\right) \exp\left[-\tau\left(\sum_{s'} q_{s,s'}\right)\right]}_{\text{likelihood of a trip arriving by } \tau} \times \underbrace{\frac{q_{s,s'}}{\left(\sum_{s'} q_{s,s'}\right)}}_{\text{prob of transitioning to } s' | \text{ a trip arrives}} = q_{s,s'} g(\tau, s; \mathbf{q}).$$

In the second case, the interval τ is right-censored by either a charging event or the conclusion of the driver's observation period, as shown below:

Case 2:



Its likelihood corresponds to the probability that no trip arrives during this interval, which is given by $g(\tau, s; \mathbf{q})$.

Now consider a sample of M drivers, each experiencing N_m state transitions in the sample. Let $\tau_{mn} \equiv \underline{t}_{mn} - \bar{t}_{m,n-1}$ denote the time interval between the completion of the previous event and the beginning of the next event (a trip, charging, or end of the observation period). Define $\mathbb{1}_{mn}(\text{Trip}, s')$ as the indicator for whether the n-th transition for driver m is a trip ending in state s', and $\mathbb{1}_{mn}(\text{Chg}, \bar{s}) = 1$ if the n-th transition is a charging event that restores battery to its full capacity, $\bar{s}$, or if the interval is right-censored by the termination of the observation window (in which case $\bar{s}$ is the same as the state of the last event). The log-likelihood of the

observed transition processes is:

$$LL1(\mathbf{q}) = \sum_{m=1}^{M}\sum_{n=1}^{N_m}\left[\underbrace{\sum_{s'}\mathbb{1}_{mn}(\text{Trip}, s')\left[\ln g(\tau_{mn}, s_{mn}; \mathbf{q}) + \ln q_{s,s'}\right]}_{\text{Case 1}} + \underbrace{\mathbb{1}_{mn}(\text{Chg}, \bar{s})\ln g(\tau_{mn}, s_{mn}; \mathbf{q})}_{\text{Case 2}}\right].$$

We use $\hat{\mathbf{q}}$ to denote the MLE estimate of the exogenous transition process, where the relevant parameters are specified in Equation (4).

Estimating Structural Parameters Given structural parameters in trip utility and charging costs, $\boldsymbol{\theta} = \{\boldsymbol{\alpha}, \boldsymbol{\beta}\}$, and the state transition process estimated in the first stage, $\hat{\mathbf{q}}$, we can solve the state-dependent value function via value function iteration as defined in Equation (10): $T(V(s|\hat{\mathbf{q}}, \boldsymbol{\theta})) \to V(s|\hat{\mathbf{q}}, \boldsymbol{\theta})$.

A driver's decision to accept a trip opportunity depends on the current vehicle range r_s relative to a threshold χ. When the range is sufficient ($r_s > \chi$), the driver is assumed to always accept the trip. Otherwise, the probability of acceptance is governed by a logit specification that balances the disutility from range anxiety against the value of the trip:

$$\pi_{\text{trip}}(s, s'|\hat{\mathbf{q}}, \boldsymbol{\theta}) = \begin{cases} \dfrac{\exp[\psi(1, s, s'|\boldsymbol{\theta}) + V(s'|\hat{\mathbf{q}}, \boldsymbol{\theta})]}{\exp[\psi(1, s, s'|\boldsymbol{\theta}) + V(s'|\hat{\mathbf{q}}, \boldsymbol{\theta})] + \exp(V(s|\hat{\mathbf{q}}, \boldsymbol{\theta}))} & \text{if } r_s \leq \chi \\ 1 & \text{if } r_s > \chi \end{cases}$$

where χ is the range anxiety cutoff. Similarly, when a charging opportunity arises, the driver decides whether to charge based on the associated costs and the value of a full battery. The probability that a driver chooses to charge is given by:

$$\pi_{\text{chg}}(s|\hat{\mathbf{q}}, \boldsymbol{\theta}) = \frac{\exp[c(1, s|\boldsymbol{\theta}) + V(\bar{s}|\hat{\mathbf{q}}, \boldsymbol{\theta})]}{\exp[c(1, s|\boldsymbol{\theta}) + V(\bar{s}|\hat{\mathbf{q}}, \boldsymbol{\theta})] + \exp(V(s|\hat{\mathbf{q}}, \boldsymbol{\theta}))}$$

By combining the driver's decision rules with the exogenous arrival process, we can define the arrival rates for observed behaviors. Specifically, the observed trip rate is $\tilde{q}_{s,s'} = \hat{q}_{s,s'}\pi_{\text{trip}}(s, s'|\hat{\mathbf{q}}, \boldsymbol{\theta})$ and the observed charging rate is $\lambda_c\pi_{\text{chg}}(s|\hat{\mathbf{q}}, \boldsymbol{\theta})$. Given the well-known "thinning" property of a Poisson process (Ross, 1995), an independent selection from a Poisson process with probability p yields a new Poisson process with rate $p\lambda$. Hence, the observed sample of both driver-chosen trips and charging events can be characterized as a Poisson process with an updated arrival rate of $\sum_{s'}\tilde{q}_{s,s'} + \lambda_c\pi_{\text{chg}}$.

Consequently, the joint density of observing a trip acceptance leading to state s' at time τ

(following a duration of inactivity) is the product of the event-specific rate and the probability of no prior arrivals:

$$\underbrace{\hat{q}_{s,s'}\pi_{\text{trip}}(s,s'|\hat{\mathbf{q}},\boldsymbol{\theta})}_{\tilde{q}_{s,s'}} \underbrace{\exp\left[-\tau\left(\sum_{s'}\tilde{q}_{s,s'}+\lambda_c\pi_{\text{chg}}\right)\right]}_{h(\tau,s;\hat{\mathbf{q}},\boldsymbol{\theta})}$$

where $h(\tau, s; \hat{\mathbf{q}}, \boldsymbol{\theta})$ represents the survival function of the aggregate Poisson process and $\tilde{q}_{s,s'} = \hat{q}_{s,s'}\pi_{\text{trip}}(s, s'|\hat{\mathbf{q}}, \boldsymbol{\theta})$ is the effective arrival rate for that specific trip destination. Similarly, the joint density of observing a charging event at time τ is:

$$\lambda_c\pi_{\text{chg}}(s|\hat{\mathbf{q}},\boldsymbol{\theta})\exp\left[-\tau\left(\sum_{s'}\tilde{q}_{s,s'}+\lambda_c\pi_{\text{chg}}\right)\right]$$

For each driver m and observed action $n = 1, ..., N_m$, we define $I_{mn}(\text{Trip}, s') = 1$ if the event is a trip to state s', and $I_{mn}(\text{Chg}, \bar{s}) = 1$ if the event is a charging session that restores the battery to full capacity. The second stage log-likelihood function is:[26]

$$LL2(\boldsymbol{\theta}) = \sum_{m=1}^{M}\left[\sum_{n=1}^{N_m}\Bigg(\underbrace{\ln h\left(\tau_{mn}, s_{mn}; \hat{\mathbf{q}}, \boldsymbol{\theta}\right)}_{\text{Common term to trips and charging}} + \underbrace{\sum_{s'} I_{mn}(\text{Trip}, s')\ln\pi_{\text{trip}}(s_{mn}, s'|\hat{\mathbf{q}}, \boldsymbol{\theta})}_{\text{trips}}\right.$$
$$\left.+\underbrace{I_{mn}(\text{Chg}, \bar{s})\ln\pi_{\text{chg}}(s_{mn}|\hat{\mathbf{q}}, \boldsymbol{\theta})}_{\text{charging}}\Bigg) + \underbrace{\ln h\left(\tau_{m,N_m+1}, s_{m,N_m+1}; \hat{\mathbf{q}}, \boldsymbol{\theta}\right)}_{\text{Terminal interval}}\right],$$

where τ_{m,N_m+1} denotes the interval between the last event and the end of the observation period and s_{m,N_m+1} denotes the final state. Because the Poisson process is memoryless, the likelihood depends only on observed transitions and the durations between them, remaining independent of unobserved opportunities that were not taken. We estimate the parameter vector $\boldsymbol{\theta} = \{\boldsymbol{\alpha}, \boldsymbol{\beta}\}$ using Maximum Likelihood Estimation (MLE).

[26] We solve for the value function for each driver type, derive the log-likelihood for drivers in each type, and then sum over all types in $LL2(\boldsymbol{\theta})$.

4 Estimation Results

4.1 Model Estimates

Trip Arrival Rates Since drivers with access to home charging, i.e., slow charging at home or workplace, may exhibit different vehicle usage from those without, we report trip frequencies and state transition probabilities separately for the two groups in Table 2. We begin with drivers without access to home charging, who make up 67% of the drivers, and then present corresponding statistics for those without a home charger. Overall, the trip patterns across the two groups appear qualitatively similar, though drivers with home chargers are more likely to take trips that end in areas with lower charging density.

The top panel of Table 2 summarizes the estimated daily Poisson arrival rates of trips by distance. As described in Section 3.1, since range anxiety is irrelevant when the remaining battery range exceeds 300 km, we use trip frequencies observed in these high SOC states to estimate the exogenous arrival rates of trips with different distances, $\{\lambda_0, ..., \lambda_9\}$. The estimates show a clear pattern: short trips are much more frequent than long-distance ones. Among drivers without a home charger, trips under 50 km occur on average 2.83 per day, while trips of 50–100 km occur 1.25 times per day. In contrast, trips longer than 200 km are infrequent, with arrival rates falling below 0.04 per day. This pattern is consistent with observed EV usage: most trips are for daily commuting or errands, while long-distance travel is occasional due to range constraints, planning needs, and limited charging infrastructure. Trip arrival patterns are similar for drivers with home chargers.

Trip Transition Frequencies The bottom three panels of Table 2 document the empirical frequencies of trips ending in destinations grouped by quartiles of charging access and charging prices, separately for 2021 and 2024. In 2021, a larger share of trips ended in areas with low charging access, reflecting the uneven early development of the charging network. By 2024, trips were more likely to end in locations with high charging access, suggesting a more developed charging infrastructure across the city.

Appendix Table A4 also reports trip arrival rates separately for daytime and nighttime, along with amenity differences across destinations. Trip activity is notably higher during the daytime (8AM–8PM), averaging 5.69 trips per day for drivers without a home charger and 6.30 trips for those with one. At night (8PM–8AM), average trip frequencies decline to 2.53 and 1.43 trips per day for drivers without and with home charging, respectively.

Trip Utility Parameters We present results from two specifications: the main specification and an alternative specification that allows trip arrival rates to differ between daytime and nighttime, while adding trip timing (day versus night) and amenity access as additional state variables. We discuss the results from the main specification first.

The top panel of Table 3 presents structural parameters governing the utility of taking a trip as a function of trip distance. The average base utility of a trip is captured by α_0, and the estimate from the main specification implies the average utility of a trip to be about ¥32 (or \$4.6), thus suggesting high costs of foregoing trips.[27] The positive coefficient estimate on α_1 suggests that drivers gain a larger utility from longer trips. The negative coefficient estimates on α_2 and α_3 suggest that trips leading to a low battery level generate disutility, especially for trips that would reduce the range to be below 50km. These negative estimates, capturing the extent of range anxiety, are consistent with the drop in observed trip frequencies for trips that lead to low battery levels in Figure 6.

Charging Cost Estimates The middle panel of Table 3 summarizes estimates for the cost of charging for drivers *without* home chargers. The coefficient estimate on β_0 (-2.55) suggests a large hassle (non-price) cost for undertaking fast charging, as it involves searching, parking, and waiting, especially so with limited charging access. Our estimates indicate that access to the fast stations greatly reduces the hassle cost from ¥24 to ¥13 (or \$3.5 to \$2) from the 2021 network to the 2024 network ($\beta_1 = 0.70$).We convert the charging prices and use the average charging quality $\bar{q} = 30$kWh per charging event to get the monetized hazard cost: $-\frac{\beta_0+\beta_1\times\overline{CA}}{\beta_2} \times \bar{q}$.

The coefficient estimate on β_2 (-1.48) implies that charging costs are more substantial than hassle costs for fast charging: assuming 30kWh per charge, the average hassle cost accounts for 25% to 38% of the total cost, and charging costs account for the rest. Based on the structural estimates, we can compute the elasticity of charging given a uniform increase in the charging price (in all stations) to be -0.98. These estimates are consistent with the data pattern shown in Figure 4: consumers not only value charging convenience but also are sensitive to charging prices.

The bottom panel of Table 3 summarizes estimates for the cost of charging for drivers *with* home chargers. These drivers have options of both slow charging at home or workplace and fast charging at commercial public charging stations. Consistent with the intuition, the hassle cost of home charging is close to zero ($\beta_3^h \approx 0$), but the hassle cost of charging at fast chargers

[27] We calculate the compensating variation in charging prices for an average trip value ($\alpha_0 + \alpha_1 \times \overline{dist}$). The monetized trip value is comparable to the taxi cost for a trip of about 9km during the daytime in Shanghai.

is high ($\beta_0^h = -4.46$, or ¥184 per charge, or \$26). The much larger disutility from fast charging is consistent with the data pattern that drivers with home chargers charge at home 90% of the time. Interestingly, access to fast charging only alleviates the cost slightly ($\beta_1^h = 0.06$), in sharp contrast with the much larger effect of charging access for those without home chargers ($\beta_1 = 0.69$). In terms of sensitivity to charging price among drivers with home chargers: they are less sensitive to fast charging prices ($\beta_2^h = -0.72$) than to home charging (i.e., electricity) prices ($\beta_5^h = -1.85$). This likely reflects the fact that fast charging is used only when necessary and that these drivers are less familiar with fast charging networks because they use them infrequently. Note that the price coefficient for home charging is the most negative among the three types. This is supported by the data pattern, where people most often charge at home during evening hours (after 9PM), indicating high price elasticity. Overall, for consumers with home chargers, the average elasticity of charging probability with respect to charging price is -0.90; therefore, they are less price-sensitive.

Robustness Checks The second specification in Table 3 is a more flexible specification that allows trip arrival rates to differ between daytime and nighttime while including trip timing and amenity access as additional state variables. This specification delivers similar results in terms of price elasticity and the hassle cost of charging. We find slightly lower range anxiety for trips that leave 50–100 km of remaining range, which may reflect reduced anxiety when vehicles are at lower charge levels during nighttime. We also find a positive but economically small effect of amenity access on charging utility, suggesting that amenity availability plays a relatively minor role in charging decisions.

Table A5 presents results from two additional robustness checks. The specification in column (1) discretizes the remaining range into 25 km increments (rather than 50 km) to more precisely capture range anxiety. The estimated preference parameters for post-trip remaining range follow an intuitive pattern: disutility is greatest when the remaining range is under 25 km, while coefficient estimates become smaller and statistically insignificant for ranges between 75 and 100 km. Other parameter estimates are very similar to those in the baseline specification in Table 3. The specification in column (2) incorporates additional consumer heterogeneity by splitting the sample into two groups based on the median average daily trip distance. These parameter estimates remain close to those in the main specification. In principle, with sufficiently long driving histories, each driver could be modeled as a distinct type, with the trip arrival rate estimated as the individual-specific long-term average rate. This exercise indicates that our estimates of charging and trip primitives are robust even under this highly demanding specification. Together, these alternative models demonstrate

the robustness of the key parameters that underpin the EV usage and charging decisions observed in our data.

Model fit Figure 7 illustrates the model fit by presenting trip hazard rates in Panel (a) and charging probabilities in Panels (b) and (c). Panel (a) shows that the model successfully replicates the observed pattern of missing trips at low remaining range. Panels (b) and (c) indicate that the predicted probability of charging is strongly influenced by remaining range, while charging access and charging prices shift charging probabilities in ways consistent with the data. Overall, the model's predictions closely match the observed data patterns.

4.2 Estimated Policy Functions

Figure 8 illustrates the estimated policy functions (i.e., decision rules) governing charging and travel decisions under various SOC levels and station attributes. Given that we have different consumer types, Panel (a) starts by reporting the policy functions for drivers with a maximum range of 500km, without home chargers (only relying on commercial fast chargers), and facing the 2024 charging network. Panel (a) shows that the probability of charging declines as the remaining range increases. At the same time, the charging decision is shifted by both station access and charging price: drivers are most likely to charge when there is better access to charging network and when prices are low (orange dashed line on the top), and least likely when stations are sparse and prices are high (yellow dashed line on the bottom). This confirms the important role of charging access and charging price in charging decisions, consistent with the data pattern shown in Figure 4.

Panel (b) extends the analysis by comparing charging probabilities across consumers with different maximum ranges. The curves are closely aligned, suggesting that the general shape of the charging policy is preserved across EVs with different maximum ranges. However, vehicles with a larger maximum range is less likely to charge given the same SOC (in % of maximum range), indicating the advantage of a larger battery.[28] But they are more likely to charge given the same remaining range (in km) because of the higher continuation value of recharging the bigger battery.

Panel (c) plots the probability of fast charging, analogous to Panel (a), but for drivers with home chargers. These drivers are very unlikely to charge at commercial fast charging stations when remaining range is high ($>$ 200km) because home charging serves as a backup

[28]For example, a car with maximum range of 500km is less likely to charge when the remaining range is 250km (50%) compared to a car with maximum range of 400km and remaining range of 200 km (50%).

option. They are also less sensitive to charging access and fast charging prices, likely because they use these stations infrequently and only in rare or urgent situations.

Panel (d) shows the probability of home charging for drivers with home chargers. The decision rules differ markedly from those for fast charging. Because home charging is convenient and involves lower hassle costs, drivers often choose to charge even when remaining range is high. Nevertheless, they are sensitive to home charging prices, with a higher likelihood of charging under off-peak prices than under peak prices.

Appendix Figure A9 presents the estimated probability of taking certain trips as heat maps. Each cell reports the conditional probability of taking a trip that changes remaining range from the value on the x-axis to the value on the y-axis, holding other location attributes fixed. Panel (a) considers trips from the most attractive origins (low prices, high access) to the least attractive destinations; probabilities are close to zero at low remaining range, indicating pronounced range anxiety under poor charging conditions. Panel (b) reverses the direction, from the least attractive to the most attractive locations, and shows high probabilities even at very low remaining range, consistent with observed travel toward cheaper and better-served areas when remaining range is low. Overall, the estimated policy responds strongly to both remaining range and spatial variation in charging prices and access.

5 Quantification and Policy Simulations

We evaluate counterfactual improvements in driving range and charging infrastructure by monetizing the model's value function, which represents the lifetime utility of vehicle usage. Specifically, we analyze two primary policy levers: battery capacity and the scale of the public charging network. Consumers' willingness to pay (WTP) for these improvements arises through three primary channels: (1) the facilitation of trips that were previously infeasible or forgone, (2) a reduction in charging hassle costs, and (3) optimized charging behavior, which reallocates charging to more cost-effective and accessible locations. Furthermore, we quantify "range anxiety" as the monetary value of forgone but feasible trips, a metric determined by both vehicle range and network coverage. Finally, we evaluate optimal policy design by integrating these welfare gains with cost data for battery and infrastructure investments.

5.1 From Value Function to WTP

To quantify consumer WTP, we analyze the value function for a vehicle with full range $\bar{R}$, given a charging network size N and home-charging access H: $V(s; N, \bar{R}, H)$. This function is

evaluated at the steady state of a continuous-time Markov process.[29] Let $\pi(s)$ represent the stationary distribution, which denotes the probability of the system occupying state s at any given time:

$$V = \sum_s \pi(s)V(s)$$
$$\text{where } \boldsymbol{\pi} \times \mathbf{Q} = \boldsymbol{\pi},$$

where $\mathbf{Q}$ is the transition rate matrix, which depends on trip rates $\tilde{\mathbf{q}}$ and charging rates $\mathbf{h}$.[30] Finally, we numerically simulate $\frac{dV}{dp}$ to translate shifts in the value function into monetary terms. By computing $\Delta p = \Delta V / \frac{dV}{dp}$ at the steady state, we express these changes as equivalent adjustments in charging prices. If the equivalent adjustment, defined here as the compensating variation, of a policy change is Δp, the resulting impact on lifetime charging costs is expressed as:

$$\text{WTP} = \Delta p \cdot \frac{D_{\text{lifetime}}}{\bar{E}}, \tag{12}$$

where $\bar{E}$ represents the average energy efficiency (6 km/kWh) and D_{lifetime} denotes the total lifetime driving distance (160,000 km), calculated based on an eight-year vehicle lifespan at 20,000 km per year. This formulation enables the translation of marginal price adjustments into a measure of lifetime WTP.

Decomposition Exercise We begin with a decomposition exercise to quantify the evolution of WTP for an EV in Shanghai from 2018 to 2024. This change is primarily driven by two factors: (1) the expansion of charging infrastructure, with the charging access measure increasing from 2.08 to 2.84, and (2) the improvement in driving range from about 350 km to 400 km. Importantly, range improvements do not apply retroactively; while legacy vehicles purchased in 2018 do not benefit from newer battery technology, they still gain utility from the expanding charging network. Due to the exponential growth of EV sales in Shanghai, pre-2018 vehicles comprised only 13% of the 2021 market, and pre-2021 vehicles accounted for just 20% of the 2024 market. Consequently, the welfare gains for the average car in the 2024 stock are comparable to, though slightly lower than those for vehicles purchased between 2021 and 2024. In the main text, we focus on the aggregated welfare changes in Figure 9, while a

[29] For notational simplicity, we denote the type-specific value function as $V(s)$.

[30] In a continuous-time Markov process, the transition rate matrix Q describes the rates of movement between states. The off-diagonal elements $q_{ij} \geq 0$ represent transition rates, while diagonal elements are defined as $q_{ii} = -\sum_{j \neq i} q_{ij}$, ensuring each row sums to zero.

detailed disentanglement of stock and flow vehicles is provided in Appendix Figure A10.

Figure 9 illustrates the evolution of WTP from 2018 to 2024, highlighting that consumers benefit from both battery advancements and the expanding charging network. When aggregated by observed home-charging shares, the weighted average WTP reaches approximately ¥30,000 by 2024; specifically, ¥62,000 for those without home chargers compared to ¥18,000 for those with them. These gains are significantly larger for households lacking home-charging access, as they rely more heavily on public infrastructure and thus benefit more from its expansion. Furthermore, these households derive greater utility from battery improvements.[31] Collectively, the total welfare improvement from 2018 to 2024 is equivalent to roughly 20% of the purchase price of an average EV.

5.2 WTP for Driving Range and Charging Access

To isolate WTP for improvement in driving range and charging access, we hold the trip arrival probabilities constant and vary the state variables to re-evaluate the value function. Regarding driving range, we increase the full range $\bar{R}$ from 250 km to 600 km in 50 km discrete intervals, a range that encompasses 95% of EVs currently on the market. To model infrastructure improvements, we induce marginal shifts in the probability distribution of regional charging access levels (ordered from lowest to highest) using the specification: $\theta_r = [0.8, 0.2, 0.0, 0.0] + [-0.1, -0.02, 0.02, 0.1] \times r$, where $r \in \{1, 2, \ldots, 8\}$. Incrementing r allows us to simulate a market's evolution from sparse to robust charging access. As a benchmark, the mean charging access levels in Shanghai were 2.08 in 2021 and 2.84 in 2024.

Panel (a) of Figure 10 reports the lifetime WTP (in ¥) for simultaneous increases in battery range and charging accessibility. The values are normalized such that WTP equals zero at the baseline of a 250 km range and a charging access index of 1.525. Three key findings emerge. First, both policy instruments exhibit significant diminishing marginal returns. Holding charging access constant at 1.525, a range increase from 250 km to 300 km raises WTP by ¥22,000, whereas an increase from 550 km to 600 km adds only ¥4,000. Similarly, with the range fixed at 250 km, improving charging access from 1.525 to 1.85 yields a gain of ¥6,000, while a shift from 3.475 to 3.80 adds only ¥4,000. Consequently, while both range and network density demonstrate diminishing marginal utility, the benefits of range extension dissipate more rapidly than those of infrastructure expansion.

Second, driving range and charging network density function as substitutes (i.e., negative

[31] Drivers without home-charging access benefit more from battery advancements because increased range reduces charging frequency, which is more costly and time-consuming for fast charging than for home charging.

cross-derivatives). From the baseline, increasing the battery range to 500 km in isolation yields ¥70,000, while increasing charging access alone to 2.825 yields ¥22,000. However, implementing both improvements simultaneously results in a total gain of ¥85,000—notably less than the ¥92,000 sum of their individual effects. Intuitively, range extensions are most valuable when charging infrastructure is sparse, whereas infrastructure improvements provide the greatest marginal utility when vehicle range is limited.

Finally, Panel (b) of Figure 10 reports the WTP for drivers with home-charging access. While the WTP for incremental improvements in range and public infrastructure is higher for those reliant on fast charging, the baseline utility for drivers with home chargers is ¥10,000 higher. This disparity underscores the significant role of residential charging in EV adoption.[32]

5.3 Quantifying Range Anxiety

In this section, we quantify the magnitude of range anxiety in monetary terms, specifically capturing the utility loss associated with forgone trips, those that are technically feasible but not undertaken due to the fear of battery depletion before reaching a charging station. In the trip utility specification defined in Equation (5), the parameters α_2 and α_3 represent the disutility of embarking on trips that result in a low state of charge. We compute the welfare impact of range anxiety as the difference in the value function between the baseline model and a counterfactual scenario where $\alpha_2 = 0$ and $\alpha_3 = 0$. In this counterfactual, we assume all feasible trips are taken, thereby isolating the utility costs driven by the psychological or risk-averse constraints of the charging state.

Figure 11 plots (monetized) range anxiety against the full driving range of the EV observed in the data for 2021 and 2024 separately. There is strong negative relationship between range anxiety and the driving range of an EV. For an EV with a driving range of 200km in 2021, the lower end of the range distribution, range anxiety amounts to ¥44,000 (or 44% of the EV price), but range anxiety reduces to only ¥3000 for an EV with a driving range of 450km. The comparison between 2021 and 2024 shows range anxiety shifts down for an EV of the same range from 2021 to 2024 due to improvement in charging access. On average, range anxiety amounts to ¥13,600 ($1,900), or 10% of the EV price in 2021. In 2024, range anxiety drops to ¥8,400 ($1,200), or 6% of the EV price. The reduction was driven by both the increase in EV driving range (from 353km to 388km), and the charging network size (from 400 to 2,268

[32]This likely represents a lower bound, as home-charging users in our sample tend to drive less frequently. If trip arrival rates were held constant across both cohorts, the implied WTP gain from home-charging access would be substantially higher.

stations), with the former contributing to 80% of the drop in range anxiety.

To further illustrate the role of charging access in affecting range anxiety, the two dotted lines depict the level of range anxiety assuming the EV of a certain driving range only has the worst charging access (top) or the best charging access (bottom) observed in the data. Consistent with the intuition, charging access plays a bigger role for EVs with a low driving range. For EVs with a range of 200km, improving charging access from the worst to the best can reduce range anxiety from ¥46,000 to ¥30,000, a 35% reduction.

Figure A11 presents range anxiety with respect to driving range separately for two groups of EV drivers: those without access to home charging in panel (a), and those with access in panel (b). Panel (a) shows that range anxiety shifts down from 2021 to 2024 for an EV with the same driving range, due to the improvement in charging access. However, there is no visible shift in range anxiety from 2021 to 2024 for those with home charging as shown in Panel (b), suggesting a more limited role of access to public charging in addressing range anxiety for those drivers with access to home charging. Comparing the two panels, average range anxiety does not differ significantly between these two groups of EV drivers due to a combination of two countervailing forces: (1) access to home charging relieves range anxiety; and (2) those with access to home charging tend to be less sensitive to overall charging prices, as the parameter estimates suggest.

Our estimates of range anxiety likely represent lower bounds of its true magnitude for two reasons. First, the EV driving data do not include inter-city travel, which tends to involve longer distances and may induce greater range anxiety. However, inter-city travel by private car is less common in China than in the U.S. due to the extensive and affordable high-speed rail network (Fang et al., 2025), and Shanghai is a major hub with direct connections to all nearby major cities. Second, our sample includes only EV drivers. Because these individuals have already chosen to purchase an EV, their range anxiety is likely lower than that of non–EV owners. Nevertheless, EVs accounted for about one-third of the passenger vehicle stock and nearly half of new vehicle sales in Shanghai by 2024.

5.4 Policy Design

Our analysis of range anxiety highlights two key remedies for mitigating it and, in turn, promoting EV adoption: increasing vehicle driving range and expanding the charging network. While countries such as China and Norway have invested heavily in charging infrastructure, the United States has lagged behind, and a large-scale build-out comparable to those countries

is unlikely in the near term.[33] In the absence of strong government support for charging infrastructure, many industry experts argue that increasing vehicle driving range is the most logical path for the next stage of EV adoption. Our following simulations aim to shed light on different approaches to promoting EV adoptions via increasing consumers' WTP. Specifically, we solve for the optimal combination of EV driving range and charging network size from the social planner's perspective. We then compare this optimal design with observed levels, as well as with the optimal outcome under a constrained scenario in which only one approach is employed. While the analysis is conducted in the context of Shanghai and the quantitative findings are unlikely to generalize to other regions, the underlying mechanisms and qualitative insights should have broader applicability.

The Value of Battery Capacity To validate the model's empirical estimates, we perform a heuristic comparison between the marginal economic benefit of extended driving range and the associated costs of increasing battery capacity.[34] A reasonable model should produce a lifetime WTP for additional range that is of a comparable order of magnitude to the physical cost of the required battery hardware. According to Barwick et al. (2025b), battery pack costs were approximately \$155/kWh in 2021 and \$115/kWh in 2024. Assuming a constant efficiency factor of $\bar{E} = 6$ km/kWh, a 50-km range extension necessitates an additional battery expenditure of approximately $50 \times (\$155/\bar{E})$ (¥9,042) in 2021 and $50 \times (\$115/\bar{E})$ (¥6,708) in 2024. These figures likely represent a lower bound for the total cost of range extension, as they exclude auxiliary expenses related to structural redesign and energy management systems.

Nevertheless, these cost estimates align closely with the WTP for a 50-km range increase derived from our model (Figure 10). Specifically, in 2021, assuming a baseline range of 350 km and a charging access level of 2.08, the estimated WTP for a 50-km increase was about ¥12,000 for households without home charging and ¥9,000 for those with it. By 2024, at a baseline range of 390 km and improved charging access at 2.84, these WTP values shifted to about ¥9,000 and ¥6,000, respectively. The alignment between these market-based costs and our model's WTP estimates provides support for the model's validity.

[33] The Bipartisan Infrastructure Bill passed in 2021 under the Biden administration allocated \$7.5 billion to expand the national charging network, but only a small fraction of the funding had been obligated due to administrative and program-approval delays prior to the start of the Trump administration, which subsequently suspended future funding.

[34] While range may also be extended through enhancements in vehicle efficiency, aerodynamics, or thermal management, these factors are held constant in this analysis. We focus exclusively on battery capacity as the primary driver of range extension, treating other technological improvements as incremental and outside the current scope.

The Value of Charging Network Expansion We evaluate the marginal economic benefit of expanding the charging network by examining the impact of adding a single station. To quantify this, we derive the mapping from the total network size to charging access, denoted as $N \rightarrow CA$, based on the observed expansion trajectory of the charging infrastructure in Shanghai (see Appendix Figure A12 for details). At a given network scale N, the marginal contribution of an additional station is defined by the gradient $\frac{\partial CA}{\partial N}$. Consequently, the WTP for one additional station can be decomposed using the chain rule: $\frac{\partial V(\bar{R},N)}{\partial N} = \frac{\partial CA}{\partial N} \cdot \frac{\partial V(\bar{R},CA)}{\partial CA}$, where $V(\bar{R}, CA)$ represents the value function associated with a given range $\bar{R}$ and access level CA.

The cost of adding one station is estimated using industry benchmarks.[35] According to these data, the unit cost per charger was approximately ¥231,000 in 2018, declining to ¥150,500 by 2024. For our baseline calculations, we assume a representative station configuration of 20 chargers. To internalize these costs at the individual level, we distribute the total station cost across a potential adoption base of one million EV drivers. These cost-benefit parameters allow us to characterize the socially optimal density of charging infrastructure for different types of consumer.

Optimal Network size and Driving Range. We solve the following optimization problem to compute the optimal level of driving range ($\bar{R}$, via charging battery capacity) and the network size (N) for different years given the associated cost and benefit parameters discussed above:

$$\max_{\bar{R},N} WTP(\bar{R}, N) - \text{Battery Cost}(\bar{R}) - \text{Charger Cost}(N). \tag{13}$$

Table 4 and Figure 12 present the optimal levels of driving range and charging network size, along with the corresponding social welfare and consumer WTP, for the years 2018, 2021, and 2024. These values are disaggregated by consumer type: those with and without access to home charging. We find that the substantial cost reductions observed between 2018 and 2024 drive a monotonic increase in the optimal levels of both driving range and network density. The optimal expansion path (indicated by the green line in Figure 12) represents the weighted average of the optimal trajectories for drivers with home chargers (red line) and those without (blue line). Specifically, the optimal combination of range and network scale $(\bar{R}, N)$ progresses from (321 km, 414 stations) in 2018, to (404 km, 825 stations) in 2021, and finally to (469 km, 1158 stations) in 2024. These results suggest that as technology matures and costs decline,

[35]The cost parameters are sourced from industry reports available at: "The Rise of 800V High-Voltage Architecture: Coordinated Upgrading Across Materials and Vehicle-Side Supply Chains", by Cinda Security, December 2022.

the social planner should shift toward a regime of both higher-capacity batteries and more ubiquitous public charging infrastructure.

Comparing the optimal benchmarks with observed market levels, we find that while Shanghai lagged in both dimensions in 2018, it has since experienced a rapid convergence, particularly regarding the charging network. The observed expansion trajectory (indicated by the dashed black line in Figure 12) reveals that the current network size has surpassed the optimal level for both consumer segments.[36] Conversely, the observed average driving range (382 km) is still far below the social optimum of 469 km. We estimate that the welfare loss, defined as the gap in social surplus between the observed state and the social optimum, is approximately ¥4,600 per consumer.

Both driving range and charging network size can reduce range anxiety, and increase consumer WTP for an EV. They are substitutes in that an arbitrarily large battery could eliminate the need for public charging, and an extremely dense network would offset limited range. However, there exists diminishing return to each technology as shown in Figure 10. This relationship implies that a coordinated investment strategy is likely to be more efficient than a singular focus on either technology. Figure A13 provides a stylized illustration of this logic: the efficient trajectory from current infrastructure and battery levels toward the social optimum is a balanced expansion path which necessitates simultaneous investment in both technologies. A one-dimensional approach, by contrast would result in efficiency losses.

Table 5 empirically evaluates the optimal expansion path of $(\bar{R}, N)$ relative to the observed trajectory and alternative strategies that prioritize only a single technology. The results indicate that focusing exclusively on either driving range or network expansion yields lower social welfare. Taking 2021 for example, both the observed range and network size (353 km, 400 stations) were below the socially optimal levels (404 km, 825 stations). In a second-best scenario, investing in range alone would require an increase to 411 km to compensate for the below-optimal charging network. Similarly, investing in the charging network alone would require 884 stations to compensate for the range deficit. While either isolated strategy would improve social welfare relative to the observed baseline (by ¥2,000 and ¥1,400 per EV, respectively), the optimal strategy of simultaneous investment increases the welfare gain by at least 50%. This effect is even more pronounced in 2024, where the welfare improvement from joint investment more than doubles the gains realized from single-technology interventions. These results underscore the complementarity in returns on investment between driving range and charging infrastructure.

[36] For context, Shanghai possessed nearly 2,300 public fast charging stations by the end of 2024, significantly outnumbering the approximately 800 gasoline stations in the city.

6 Conclusion

Although range anxiety consistently emerges as a key barrier to EV adoption in consumer surveys, industry reports, and policy discussions, there has been limited economic analysis quantifying its magnitude and evaluating the effectiveness of potential remedies. This study provides, to our knowledge, the first analysis to micro-found range anxiety, defined as the utility loss from unrealized yet feasible trips due to fear of battery depletion before reaching a charging station. We operationalize this concept by developing and estimating a continuous-time dynamic model of EV driving and charging behavior.

Leveraging high-frequency data from 8,000 EVs in Shanghai, we identify compelling evidence of range anxiety by documenting a robust pattern of "missing trips", feasible but foregone trips when such trips will result in low remaining range after travel. This behavioral distortion is more pronounced in regions with sparse charging infrastructure from IV regressions. But such a pattern does not exist for PHEVs which have auxiliary gasoline engines, further alleviating the concerns for unobserved factors. Our structural analysis estimates the average range anxiety to be approximately \$1,900 per vehicle in 2021 (about 10% of the average EV purchase price), declining to \$1,200 (6% of the average price) by 2024. These aggregate figures, however, mask substantial heterogeneity across EV models with varying driving range. The observed 37% reduction in average range anxiety over this period is primarily attributable to the rapid expansion of the charging network (from 400 to 2,268 stations) and, more significantly, to the concurrent improvement in average driving range from 353 km to 388 km.

Our simulations highlight the crucial roles of two approaches in addressing range anxiety: expanding driving range (through increased battery capacity) and enhancing charging access (through larger charging networks). Because each approach exhibits diminishing returns, the optimal policy requires coordinated investment in both charging infrastructure and battery capacity. The socially optimal levels of charging network size and driving range evolve as the costs of charging station construction and battery production decline over time. Our analysis indicates that the realized investment trajectory diverges significantly from the optimal path: by 2024, Shanghai has over-invested in charging infrastructure while under-investing in driving range relative to the social optimum.

We note two important caveats and directions for future research. First, our data and analysis are restricted to travel within Shanghai, and thus our estimates of range anxiety likely represent a lower bound, as range anxiety may be more pronounced for long-distance trips. That said, long-distance driving is less common in China than in countries such as the U.S., partly due to China's extensive high-speed rail system. Second, our empirical analysis

is based on data from Shanghai, and the quantitative findings should be interpreted in that context. As detailed EV usage and charging data become available elsewhere, our framework can be adapted to quantify range anxiety and its policy implications across different settings, where underlying preferences may vary. Another important direction for future research is to leverage granular data to examine the optimal spatial distribution of charging infrastructure while explicitly incorporating range anxiety in the model.

References

Arkolakis, Costas, Kenneth T. Gillingham, and Seung-Yong Yoo, "Optimizing Electric Vehicle Infrastructure," *AEA Papers and Proceedings*, May 2025, *115*, 563–67.

Bailey, Megan R., David P. Brown, Blake C. Shaffer, and Frank A. Wolak, "Show Me the Money! A Field Experiment on Electric Vehicle Charge Timing," *American Economic Journal: Economic Policy*, 2025, *17* (2), 259–284.

Barwick, Panle Jia, Christopher Knittel, Shanjun Li, Youming Liu, James Stock, and Binglin Wang, "Optimal Charging Infrastructure for Electric Vehicles," Working Paper 2025.

_ , Hyuk-Soo Kwon, and Shanjun Li, "Attribute-based Subsidies and Market Power: an Application to Electric Vehicles," Working Paper 32264, National Bureau of Economic Research March 2024.

_ , _ , _ , and Nahim B Zahur, "Drive Down the Cost: Learning by Doing and Government Policies in the Global EV Battery Industry," Working Paper 33378, National Bureau of Economic Research January 2025.

Bernard, Louise, Andy Hackett, Robert Metcalfe, Luca Panzone, and Andrew Schein, "The Impact of Dynamic Prices on Electric Vehicle Public Charging Demand: Evidence from a Nationwide Natural Field Experiment," Technical Report, Centre for Net Zero May 2025. Working Paper.

Bloomberg Intelligence, "Global Battery Electric Vehicle Outlook," 2024.

Burlig, Fiona, James Bushnell, David Rapson, and Catherine Wolfram, "Low Energy: Estimating Electric Vehicle Electricity Use," *AEA Papers and Proceedings*, May 2021, *111*, 430–35.

Bushnell, James B, Erich Muehlegger, and David S Rapson, "Energy Prices and Electric Vehicle Adoption," *Journal of Political Economy Microeconomics*, 2025.

Cabral, Luis, Chiara Gardenghi, Deepak Hegde, and Junrui Lin, "Public and Private Innovation: Complements or Substitutes?," *Columbia University Working Paper*, 2025.

Chokshi, Niraj, Matthew Goldstein, and Erin Woo, "Biden's electric car plans hinge on having enough chargers," *The New York Times*, 2021. Accessed: 2025-07-12.

Dorsey, Jackson, Ashley Langer, and Shaun McRae, "Fueling alternatives: Gas station choice and the implications for electric charging," *American Economic Journal: Economic Policy*, 2025, *17* (1), 362–400.

Fang, Hanming, Ming Li, Long Wang, and Zoe Yang, "High-Speed Rail and China's Electric Vehicle Adoption Miracle," Working Paper 33489, National Bureau of Economic Research February 2025.

Gao, Hong, "In-depth Report on the Charging Pile Industry," Tech. Rep., Nanjing Securities 2023.

Garg, Teevrat, Ryan Hanna, Jeffrey Myers, Sebastian Tebbe, and David G. Victor, "Electric Vehicle Charging at the Workplace: Experimental Evidence on Incentives and Environmental Nudges," CESifo Working Paper 11445, CESifo, Munich 2024.

Heid, Pascal, Kevin Remmy, and Mathias Reynaert, "Equilibrium Effects in Complementary Markets: Electric Vehicle Adoption and Electricity Pricing," *TSE Working Paper*, 2024.

Jacqz, Irene and Sarah Johnston, "Electric Vehicle Subsidies and Urban Air Pollution Disparities," *Journal of the Association of Environmental and Resource Economists*, 2024, *11* (S1).

Kaps, Christian, Michael W. Toffel, and Ulrich Niklas, "Are We There Yet? Evaluating the Transition to EVs," Working Paper, Harvard Business School December 2025.

Klier, Thomas H. and James M. Rubenstein, "North America's Rapidly Growing Electric Vehicle Market: Implications for the Geography of Automotive Production," *Economic Perspectives*, December 2022, *No. 5.* Accessed: 2025-07-12.

La Nauze, Andrea, Lana Friesen, Kai Li Lim, Flavio M. Menezes, Lionel Page, Thara Philip, and Jake Whitehead, "Can Electric Vehicles Aid the Renewable Transition? Evidence from a Field Experiment Incentivising Midday Charging," CESifo Working Paper 11386, CESifo, Munich 2024.

Li, Jing, "Compatibility and investment in the us electric vehicle market," *Unpublished manuscript, MIT*, 2023.

_ **and Katalin Springel**, "Entry and Coordination in the U.S. Electric Vehicle Charging Industry," *Tufts Working Paper*, 2025.

Li, Shanjun, Lang Tong, Jianwei Xing, and Yiyi Zhou, "The market for electric vehicles: indirect network effects and policy design," *Journal of the Association of Environmental and Resource Economists*, 2017, *4* (1), 89–133.

Liu, Yifan, Azell Francis, Catharina Hollauer, M. Cade Lawson, Omar Shaikh, Ashley Cotsman, Khushi Bhardwaj, Aline Banboukian, Mimi Li, Anne Webb, and Omar Isaac Asensio, "Reliability of electric vehicle charging infrastructure: A cross-lingual deep learning approach," *Communications in Transportation Research*, 2023, *3*, 100095.

Liu, Zikun, "Policy Design for Sustainable Innovation and Adoption: A Structural Analysis of the Electric Vehicle Market," 2025. Working Paper.

Qin, Molin and Jonathan Scott, "The High Cost of Low Range: Estimating the Hidden Cost of Range Anxiety in Electric Vehicles," *Journal of Industrial Economics*, 2025. forthcoming.

Rainieri, Giuseppe, Chiara Buizza, and Alberto Ghilardi, "The psychological, human factors and socio-technical contribution: A systematic review towards range anxiety of battery electric vehicles' drivers," *Transportation Research Part F: Traffic Psychology and Behaviour*, 2023, *99*, 52–70.

Rapson, David S. and Erich Muehlegger, "The economics of electric vehicles," *Review of Environmental Economics and Policy*, 2023, *17* (2), 274–294.

Remmy, Kevin, "Adjustable Product Attributes, Indirect Network Effects, and Subsidy Design: The Case of Electric Vehicles," 2025. Working Paper.

Ross, Sheldon M., *Stochastic Processes, 2nd Edition*, Wiley, 1995.

Springel, Katalin, "It's Not Easy Being "Green": Lessons from Norway's Experience with Incentives for Electric Vehicle Infrastructure," *Review of Environmental Economics and Policy*, 2021, *15* (2).

_ , "Network externality and subsidy structure in two-sided markets: Evidence from electric vehicle incentives," *American Economic Journal: Economic Policy*, 2021, *13* (4), 393–432.

Sunada, Takeaki and Tianli Xia, "From Pumps to Plugs: Value of Time and Charging Policies," *Working paper*, 2025.

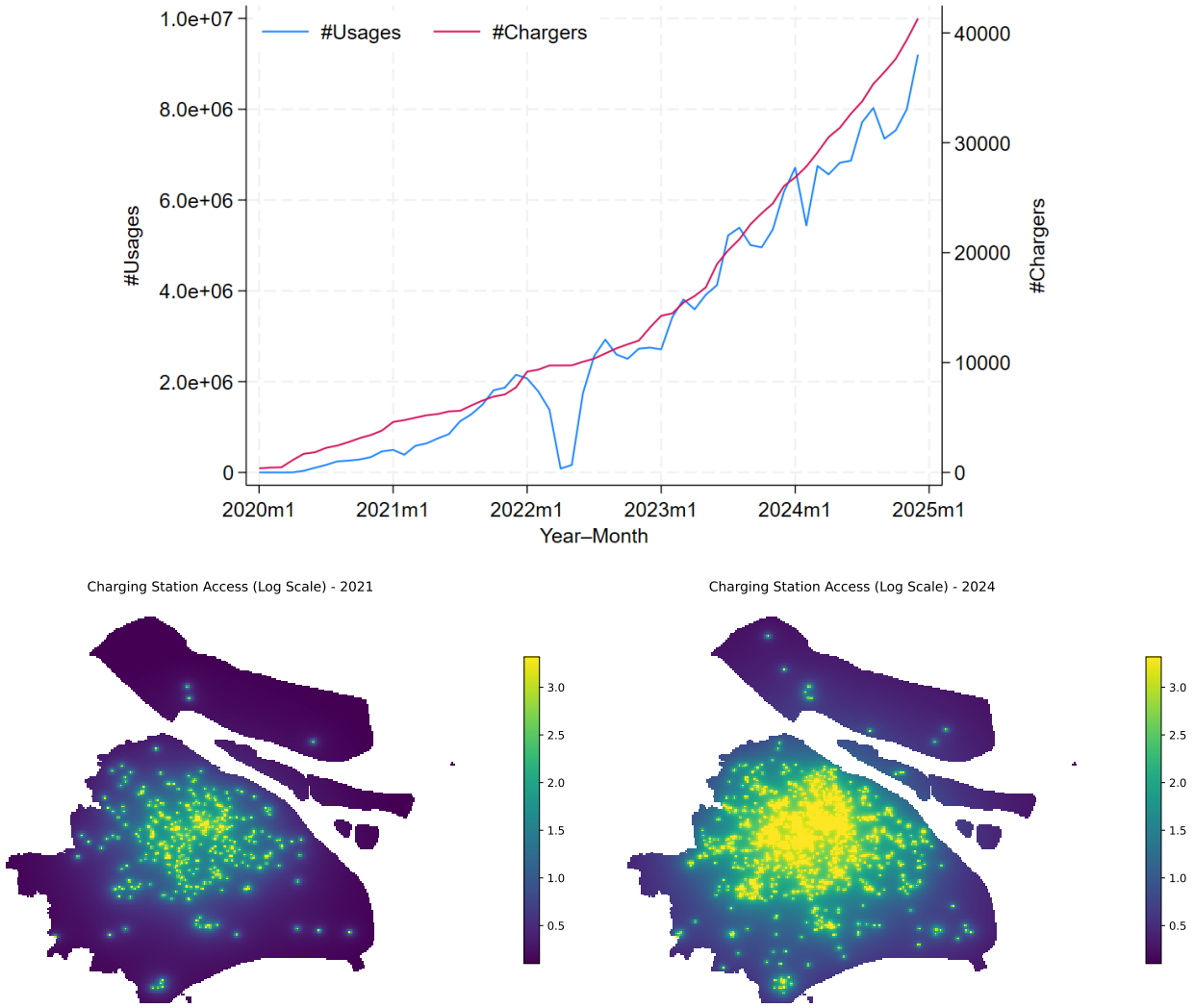
Wang, Yucheng, "Who Receives Environmental Benefits from Driving Electric Vehicles?," *Unpublished Manuscript*, April 2024.

Wardlaw, Christian, "What is Range Anxiety with Electric Vehicles?," J.D. Power November 2020. Accessed 2025-07-12.

Zhou, Yiyi and Shanjun Li, "Technology Adoption and Critical Mass: The Case of the U.S. Electric Vehicle Market," *The Journal of Industrial Economics*, 2018, *66* (2), 423–480.

Main Figures

Figure 1: Numbers and Usage of Fast-Chargers

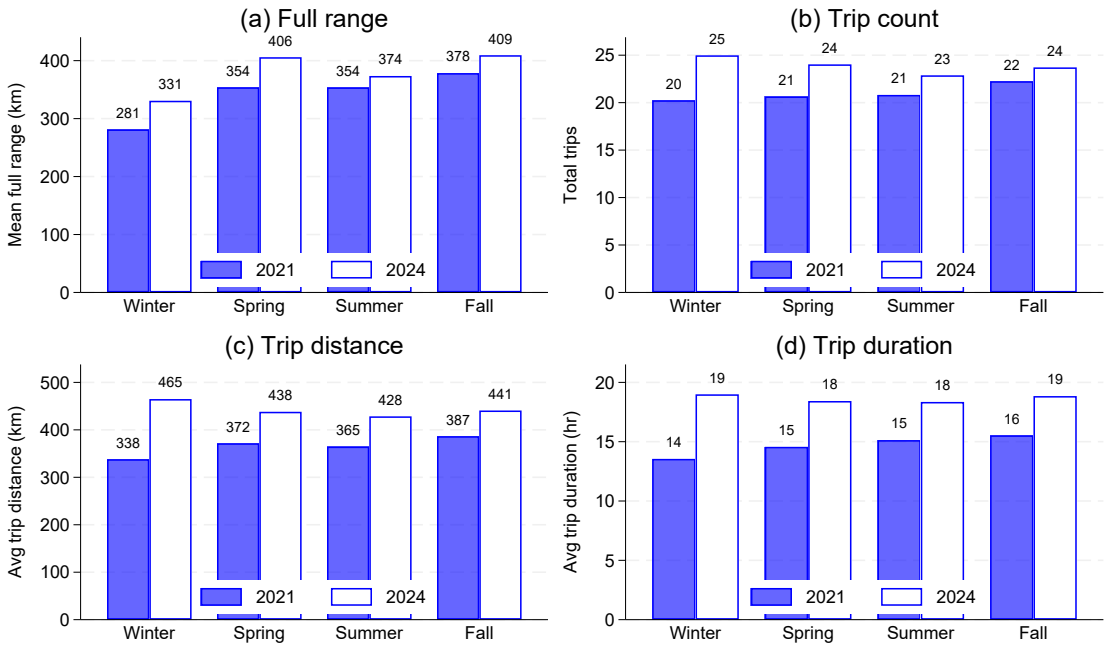


(a) Charging Access (2021)

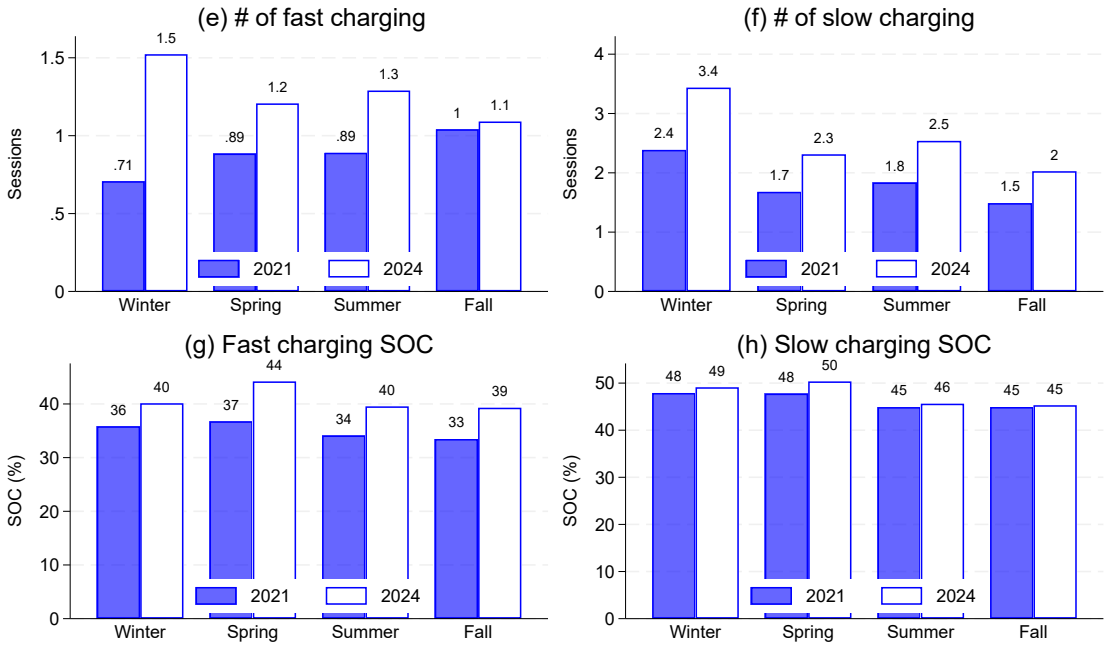
(b) Charging Access (2024)

Notes: The top figure shows the number of fast charging chargers and their usage (number of charging events) in Shanghai. There are on average 15 chargers per station. Bottom Figures (a) and (b) report the log(charging access) of each location measured in 2021 and 2024. Charging access for location i is defined as the sum of the inverse squared distance to fast charging stations i. ($CA_i = \sum_j \frac{1}{dist_{ij}^2}$).

Figure 2: Data Description of EV usage dataset: 2021 vs. 2024



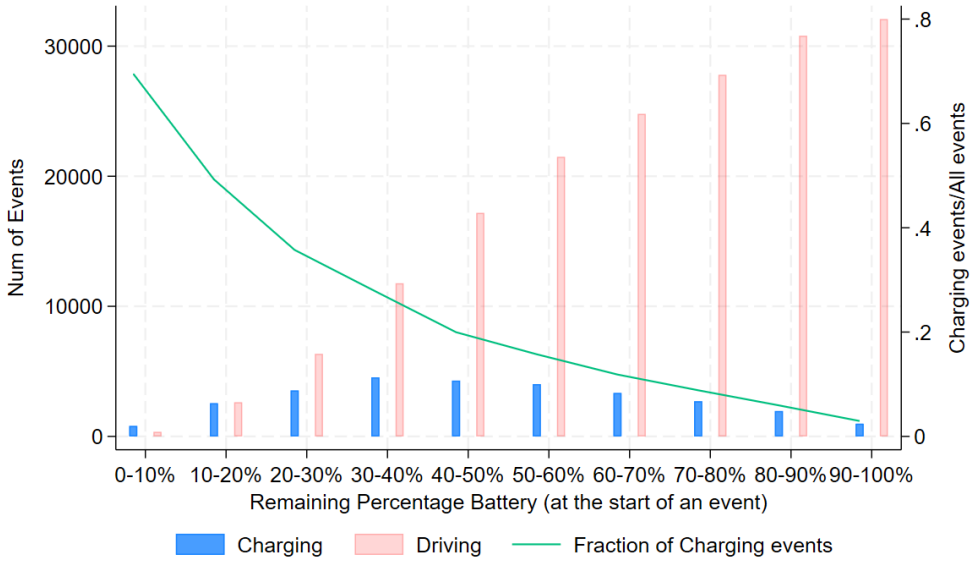
(a) Trip-related events



(b) Charging-related events

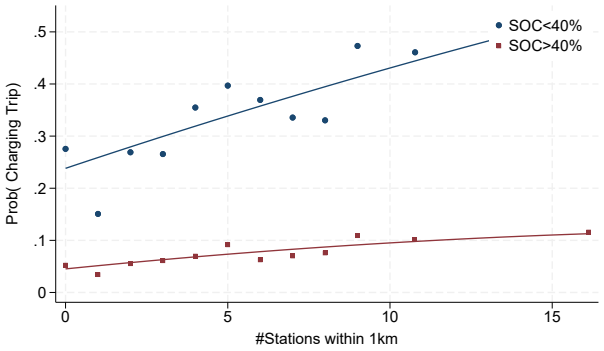
Notes: The dataset in each year includes four weekly cross-sections of 1100 randomly selected representative EVs in Shanghai during a week in Jan (Winter), March (Spring), Aug (Summer), and Oct (Fall), respectively, for the years 2021 and 2024. The top panel reports vehicle range, weekly trip count, weekly distance, and weekly trip duration. The bottom panel reports the weekly fast charging and slow charging events, as well as SOC for fast charging and slow charging, respectively.

Figure 3: Number of Events by Remaining Battery

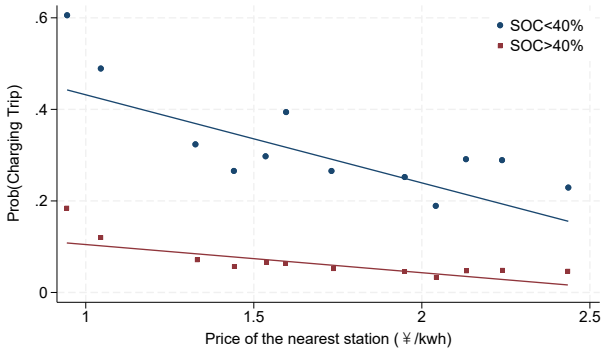


Notes: A driving event (or a non-charging trip) is defined by the start of the car to the shut-off of the car when the distance traveled is above 100 meters. A charging event includes both fast charging at stations, and home charging. For fast charging, the charging events include the travel to the charger, charging at the station, and the immediate travel away from the charging station, provided the travel is initiated within 30 minutes of the end of charging. Fraction of charging events show the ratio of charging events over charging and driving events.

Figure 4: Charging Behavior as a Function of Charging Network and Price



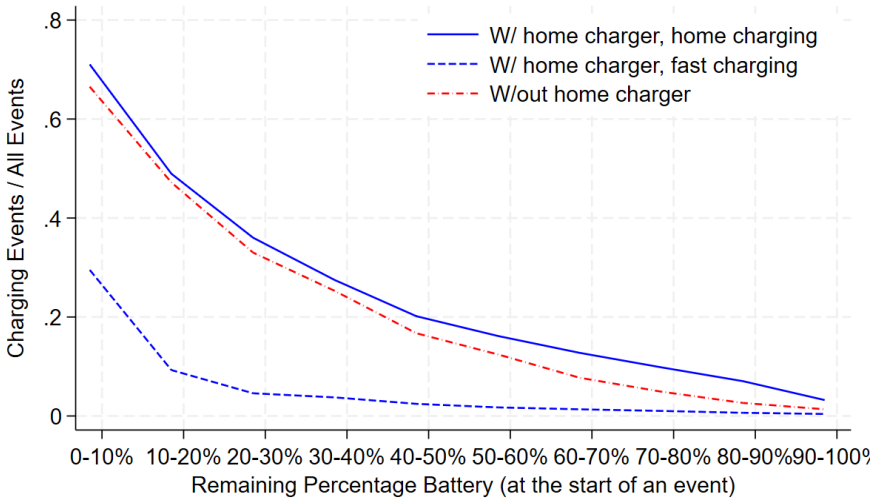
(a) Charging probability vs. local charging access



(b) Charging probability vs. price at nearest station

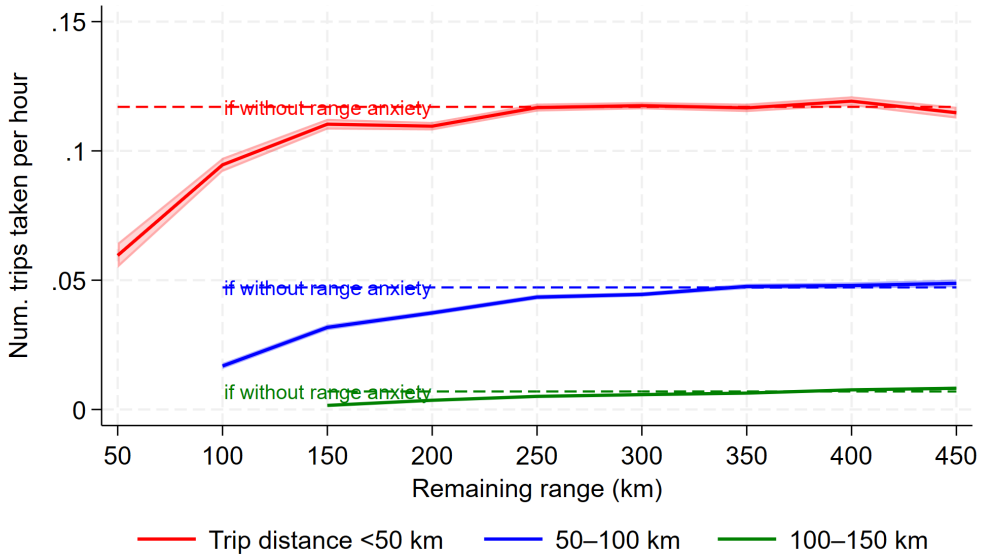
Notes: these graphs examine how charging probability varies with local station access and price. Consumers are more likely to charge in areas with a dense network (Panel (a)) and low prices (Panel (b)). In both cases, the effect is stronger when the remaining battery (SOC) is below 40%.

Figure 5: Charging behavior by remaining battery: with or without home chargers



Notes: This figure plots the distribution of charging events by the remaining percentage of battery at the start of an event. The solid blue line shows home charging for users with home chargers, while the dashed blue line indicates their fast charging behavior. The dashed red line represents users without home chargers. Charging at very low battery levels is disproportionately concentrated among those without home chargers, while users with home chargers tend to charge more frequently at higher remaining battery levels.

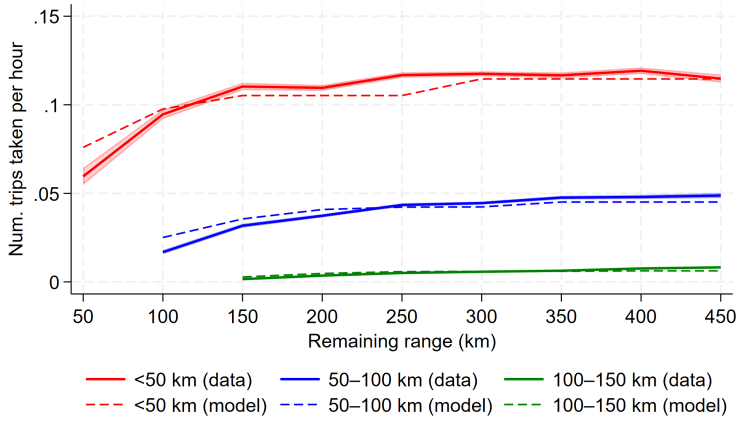
Figure 6: Range Anxiety: hourly hazard rate of trip initiation by remaining driving range



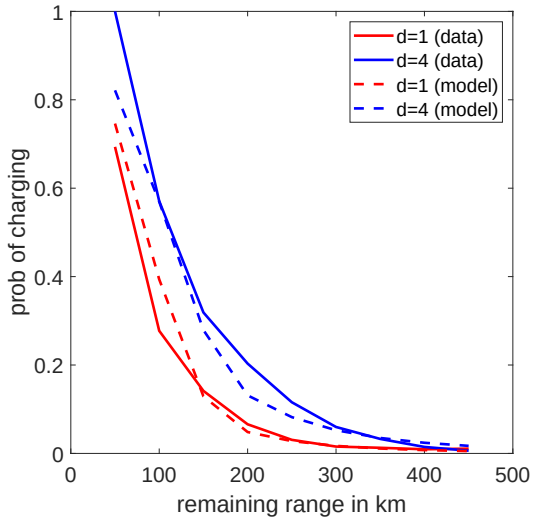
Notes: Each colored line corresponds to a trip with a certain distance: $<$ 50 km, 50–100 km, 100–150 km, and 150–200 km. Hazard rates are computed as the number of trips initiated per hour from each starting remaining range (x-axis), normalized by the hours vehicles stay in that state (until a trip arrives). Shaded areas show 95% confidence intervals.

Figure 7: Model Fit: Trip Hazard Rates and Charging Probabilities

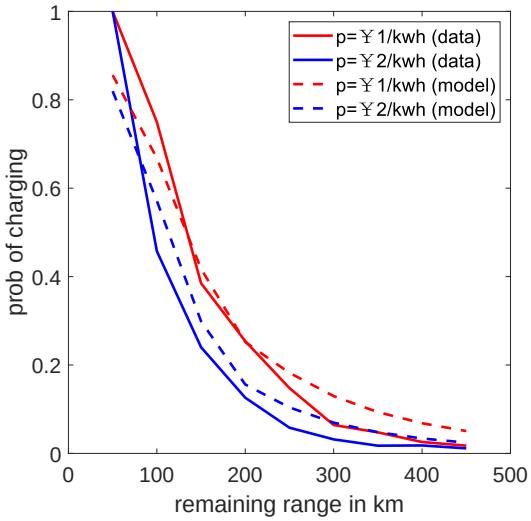
(a) Trip hazard rates by trip distance



(b) Charging decision by charging access



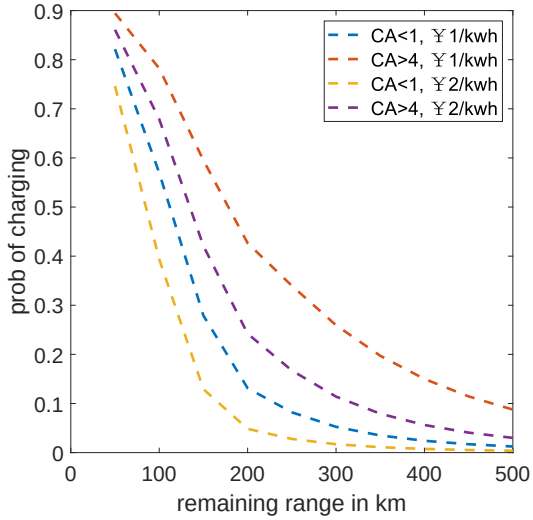
(c) Charging decision by charging price



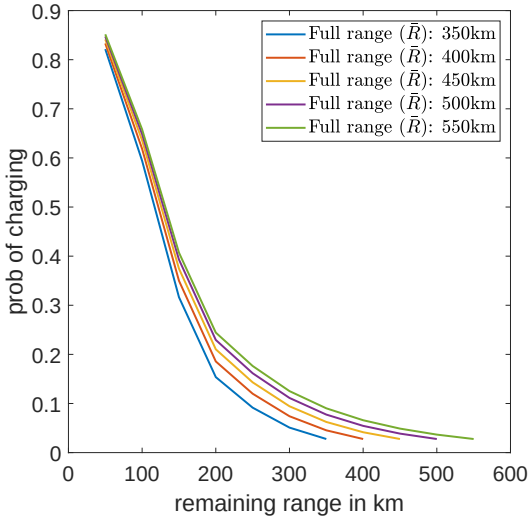
Notes: This figure demonstrates model fit for trip hazard rates in Panel (a), and charging probabilities in Panels (b) and (c). Solid lines denote data patterns and dashed line denotes model predictions.

Figure 8: Estimated policy function $h(b, d, p, h)$

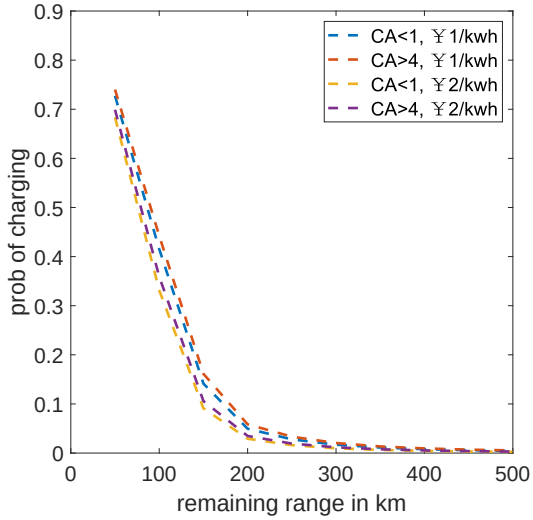
(a)$\pi^{H=0,\bar{R}=500}(r; d, p)$



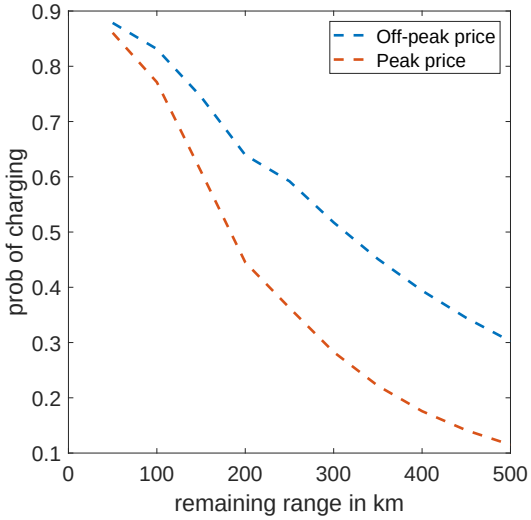
(b) $\pi^{H=0,\bar{R}}(r)$



(c) $h^{H=1,\bar{R}=500}(r; d, p, h = 0)$

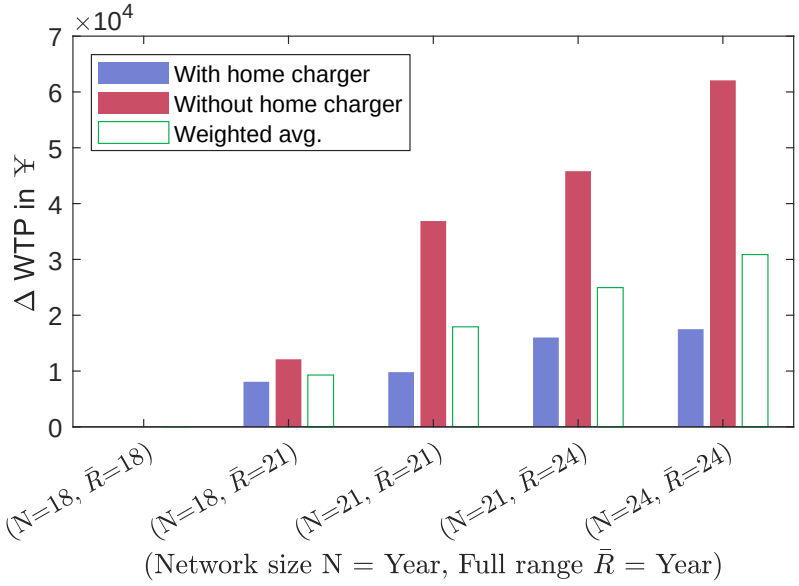


(d) $h^{H=1,\bar{R}=500}(r; d, p, h = 1)$



Notes: This figure presents the estimated policy functions $h(b, r, p, h)$ governing charging decisions as a function of b (remaining battery range), d (charging access), p (charging price), and h (home charger nearby). Panel (a) shows the charging probability for consumers without home chargers as a function of remaining range under four scenarios defined by price and station access. Panel (b) shows charging probabilities for consumers without home chargers across the different battery capacities. Panels (c) and (d) display the probability of charging for consumers with home chargers. The probability of using fast charging is low (close to zero when range $>$ 200km). Charging at home is frequent even when the remaining battery is relatively high and during off-peak hours.

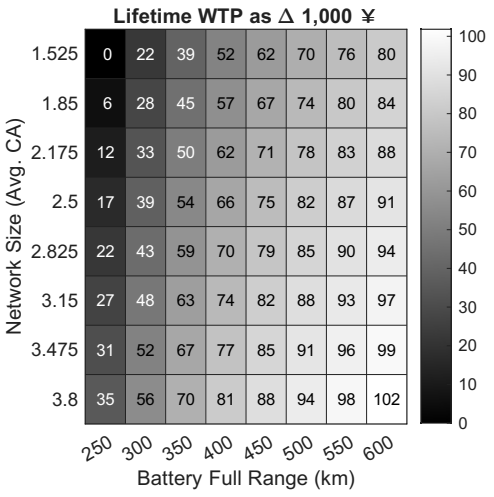
Figure 9: Decomposition of welfare gain: 2018 vs. 2021 vs. 2024



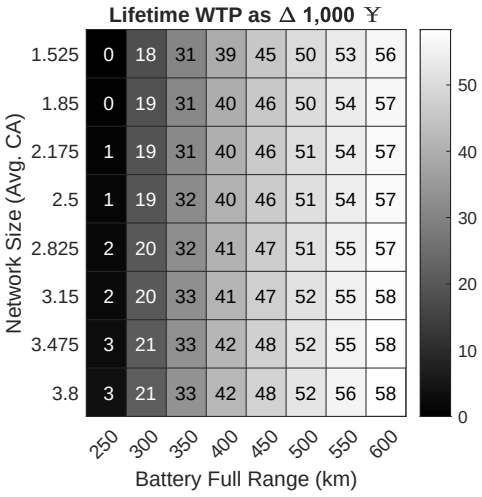
Notes: Bars show ΔWTP (lifetime WTP, 10,000 ¥) relative to 2018 (N=18, $\bar{R}$=18) as $(N, \bar{R})$ are sequentially updated to 2021 and 2024: at each x-tick, first raise $\bar{R}$ holding N fixed, then raise N holding $\bar{R}$ fixed. Colors: blue = with home charger; red = without; green = sample-weighted mean (weights = observed home-charger shares at 67%).

Figure 10: WTP for driving range and charging access

(a) Δ WTP without home chargers

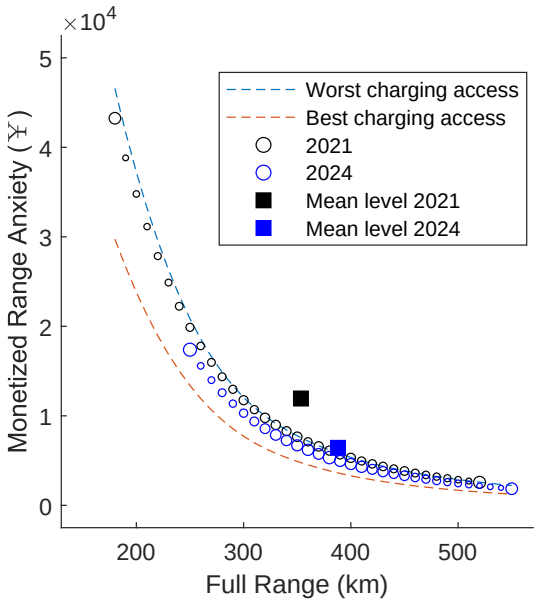


(b) Δ WTP with home chargers



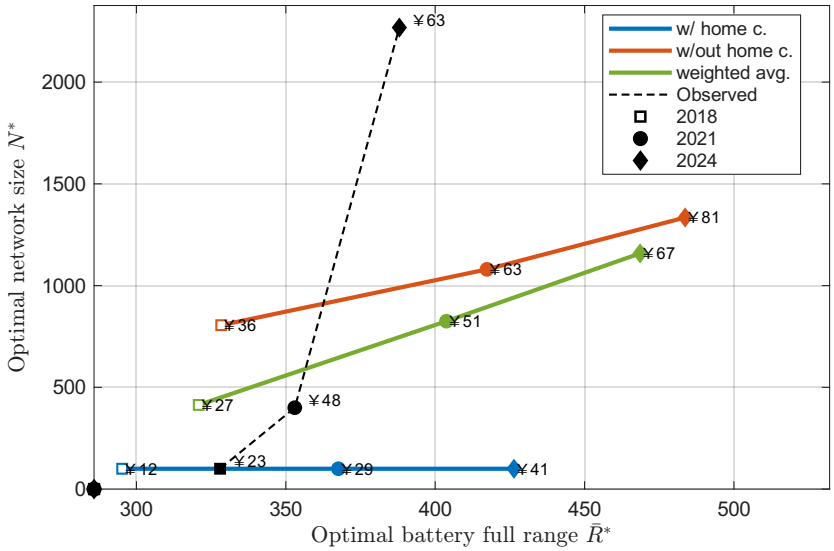
Notes: Figure (a) shows the estimated willingness to pay (WTP) for network size (or higher average charging access) and the full driving range, both expressed in terms of lifetime charging costs. The baseline in Panel (a) is 100% battery as the current level and the current charging access (CA) level. 2021 network has CA=2.08 and 2024 network has CA=2.84. Panel (b) shows the surplus loss from ("narrowly defined") range anxiety, i.e., people forgo trips that are technically feasible, computed as the difference of the value function when trips are always taken, converted to lifetime WTP.

Figure 11: Range Anxiety by Driving Range



Notes: Each panel plots *monetized range anxiety* (lifetime WTP, 10^4 ¥) against the vehicle's full range (km). Circle size is proportional to the empirical frequency of the range level in that year's EV sample. Filled squares show the weighted mean level for the year. The downward slope indicates that range anxiety declines with battery range; the downward shift from 2021 to 2024 reflects improvements in network size (from 400 to 2268 stations) and full driving range (from 353 to 388km).

Figure 12: Optimal levels of Driving Range and Charging Network Size



Notes: Each series traces the optimal pair $(\bar{R}^*, N^*)$—battery capacity (km) on the x-axis and charging-network size index on the y-axis—for three cost environments (2018, 2021, 2024). Blue: consumers *with* home chargers; orange: *without* home chargers; green: sample-weighted average (weights are the observed home-charger shares). The dashed black line connects the *observed* $(\bar{R}, N)$ in the data. Markers indicate years: □ 2018, • 2021, ◇ 2024. Currency labels next to the points report the model net surplus at the corresponding optimum (WTP minus cost, in 1,000 ¥). Connecting lines illustrate how optimal technology and infrastructure choices shift as battery and station costs change over time.

Main Tables

Table 1: Empirical Evidence of Range Anxiety

	(1) PPML	(2) PPML	(3) IV-CF
$\mathbb{1}$(Range after a trip $<$ 50km)	-0.840***	-0.879***	-0.898***
	(0.0302)	(0.0361)	(0.0410)
$\mathbb{1}$(Range after a trip $\in$ 50–100km)	-0.140***	-0.150***	-0.152***
	(0.0175)	(0.0193)	(0.0204)
$\mathbb{1}$(Range after a trip $<$ 50km) $\times$ Charging Access		0.0996***	0.162***
		(0.0329)	(0.0453)
$\mathbb{1}$(Range after a trip $\in$ 50–100km) $\times$ Charging Access		0.0387**	0.0716***
		(0.0190)	(0.0276)
Jiedao FE	Yes	Yes	Yes
Trip distance bin $\times$ Year FE	Yes	Yes	Yes

Notes: This table shows the PPML regression results from a Poisson model on the hazard rate of trips. The number of observations is 15,272 by *jiedao* (225) by year (2) by trip-bins (35). Jiedao is a sub-district administrative unit in Shanghai comparable to a census tract. The last column reports the results from the IV regression under PPML where the control function (CF) approach is implemented. The IV for charging access is constructed as the interaction between the number of points of interest (POIs) in the corresponding jiedao in 2018, and annual charging equipment costs, which drop over time. Standard errors are clustered at the jiedao level. Charging access is normalized, and one unit equals a standard deviation. The jiedao FEs, and the trip distance bin by year FEs are included.

Table 2: Model Estimates: State Arrival & Transition

	W/out H.C.		W/ H.C.	
	Estimate	SE	Estimate	SE
Trip Arrival (per day)				
<50km	2.8316	(0.0165)	2.7081	(0.0105)
50-100km	1.2479	(0.0108)	1.0021	(0.0066)
100-150km	0.2263	(0.0047)	0.1127	(0.0022)
150-200km	0.0941	(0.0030)	0.0323	(0.0012)
200-250km	0.0382	(0.0021)	0.0101	(0.0007)
250-300km	0.0193	(0.0020)	0.0037	(0.0006)
300-350km	0.0099	(0.0014)	0.0013	(0.0003)
350-400km	0.0043	(0.0013)	0.0007	(0.0004)
400-450km	0.0000	(4.1094)	0.0000	(2.3447)
Probability to a location (2021)				
Pr(->CA $\in [0,1]$)	0.4181	(0.0033)	0.5037	(0.0024)
Pr(->CA $\in [1,2]$)	0.3277	(0.0032)	0.3130	(0.0023)
Pr(->CA $\in [2,3]$)	0.1443	(0.0024)	0.1213	(0.0016)
Pr(->Price $\in [0,1.2]$)	0.2498	(0.0031)	0.2617	(0.0022)
Pr(->Price $\in [1.2,1.5]$)	0.1717	(0.0026)	0.2017	(0.0020)
Pr(->Price $\in [1.5,2]$)	0.2968	(0.0032)	0.2733	(0.0022)
Probability to a location (2024)				
Pr(->CA $\in [0,1]$)	0.1719	(0.0024)	0.2256	(0.0019)
Pr(->CA $\in [1,2]$)	0.0984	(0.0019)	0.1741	(0.0017)
Pr(->CA $\in [2,3]$)	0.2555	(0.0028)	0.2770	(0.0020)
Pr(->Price $\in [0,1.2]$)	0.2887	(0.0029)	0.2754	(0.0020)
Pr(->Price $\in [1.2,1.5]$)	0.1849	(0.0025)	0.2272	(0.0019)
Pr(->Price $\in [1.5,2]$)	0.2700	(0.0029)	0.2471	(0.0019)
Probability to home charger				
Pr(->W/ Private Charger)	-	-	0.1985	(0.0020)

Notes: The sample includes 8,000 drivers with 214,000 sessions. The table reports estimated Poisson trip arrival rates and transition probabilities by types (with or without home chargers, under the 2021 or 2024 network).

Table 3: Model Estimates: Structural Primitives

	(1) Main specification		(2) Day vs. night + Amenity	
Parameter	Estimate	S.E.	Estimate	S.E.
Trip utility				
α_0 (baseline trip utility)	2.4794	0.0129	3.4473	0.0264
α_1 (marginal utility per 50 km)	0.8492	0.0155	0.7842	0.0202
α_2 (anxiety: 50–100 km remaining)	-0.7866	0.0206	-0.2254	0.0198
α_3 (anxiety: 0–50 km remaining)	-1.9079	0.0372	-1.9304	0.0373
α_4 (utility from amenity)	—	—	0.0729	0.0073
Charging cost: drivers w/out home chargers				
β_0 (base cost)	-2.5790	0.0263	-4.0509	0.0267
β_1 (sensitivity to charging access)	0.6942	0.0100	0.7194	0.0100
β_2 (sensitivity to charging price)	-1.4823	0.0164	-1.4900	0.0167
β_3 (sensitivity to amenity)	—	—	0.1353	0.0057
Charging cost: drivers w/ home chargers				
when using fast charger:				
β_0^h (base cost)	-4.4177	0.0257	-4.7738	0.0274
β_1^h (sensitivity to charging access)	0.0641	0.0130	0.0510	0.0134
β_2^h (sensitivity to charging price)	-0.7196	0.0162	-0.8154	0.0172
when using home charger:				
β_3^h (base cost)	-0.2715	0.0184	-0.1650	0.0176
β_4^h (sensitivity to charging access)	-0.0087	0.0116	0.0408	0.0114
β_5^h (sensitivity to charging price)	-1.6274	0.0316	-1.5289	0.0307

Notes: The number of observations is 8,000 drivers with 214,000 sessions. Table 3 reports the estimated structural parameters that govern the charging and driving choices: Consumers without home chargers: $C(\text{charging}, s) = \beta_0 + \beta_1(\text{CA}) + \beta_2(\text{price}) + \beta_3(\text{amenity})$. Consumers with home chargers: $C(\text{charging}, s) = \mathbb{1}(\text{not home}) \times (\beta_0^h + \beta_1^h(\text{CA}) + \beta_2^h(\text{price})) + \mathbb{1}(\text{home}) \times (\beta_3^h + \beta_4^h(\text{CA}) + \beta_5^h(\text{price}))$. Utility from trips: $\psi(\text{trips}, k, s) = \alpha_0 + \alpha_1(\text{trip distance}) + \alpha_2 \mathbb{1}(b_k \in [50, 100]) + \alpha_3 \mathbb{1}(b_k \in [0, 50]) + \alpha_4(\text{amenity})$, where b_k denotes remaining range after trip. The first specification is the main specification where the second is the alternative where the trip arrival rate is seperately estimated for daytime (8AM-8PM) and nighttime (8PM-8AM) as shown in Table A4.

Table 4: Optimal Range and Network Size by Year

Cost level	$\bar{R}_{\text{opt}}$ (km)	N_{opt}	Welfare	WTP	Cost
Panel A: w/ home c.					
2018	295	100	12.3	43.2	30.9
2021	368	100	29.3	60.4	31.1
2024	426	100	41.0	69.2	28.2
Panel B: w/out home c.					
2018	328	806	35.8	86.6	50.8
2021	417	1080	62.5	110.7	48.2
2024	484	1335	80.8	122.3	41.6
Panel C: weighted avg.					
2018	321	414	26.6	69.8	43.1
2021	404	825	50.7	94.3	43.6
2024	469	1158	67.3	106.1	38.8

Notes: Panel A is for EV drivers without access to home charging while Panel B is for those with. Panel C shows the weighted average between the two groups. We use grid search to find the optimal bundle $\{\bar{R} \in [250, 600], N \in [100, 2500]\}$. Welfare, WTP, and Cost are reported in ¥1,000. The WTP and cost estimates are relative to an EV with a full range of 200km with charging access at the worst quartile. Welfare= WTP-social cost.

Table 5: Complementarity of Battery ($\bar{R}$) and Network Size (N)

Scenario	$\bar{R}$ (km)	N	Welfare	WTP	Cost
Panel A: 2018 level of battery and station cost					
A: $(\bar{R}^{opt}, N^{opt})$	321	414	26.6	69.8	43.1
B: $(\bar{R}^{obs}, N^{obs})$	318	100	22.4	60.4	38.0
C: $(\bar{R}^{opt}, N^{obs})$	327	100	22.5	63.3	40.7
D: $(\bar{R}^{obs}, N^{opt})$	318	414	26.6	68.9	42.2
Panel B: 2021 level of battery and station cost					
A: $(\bar{R}^{opt}, N^{opt})$	404	825	50.7	94.3	43.6
B: $(\bar{R}^{obs}, N^{obs})$	353	400	47.7	78.6	30.9
C: $(\bar{R}^{opt}, N^{obs})$	411	400	49.7	91.2	41.5
D: $(\bar{R}^{obs}, N^{opt})$	353	884	49.1	84.0	34.9
Panel C: 2024 level of battery and station cost					
A: $(\bar{R}^{opt}, N^{opt})$	469	1158	67.3	106.1	38.8
B: $(\bar{R}^{obs}, N^{obs})$	388	2268	62.7	97.3	34.6
C: $(\bar{R}^{opt}, N^{obs})$	461	2268	64.9	108.4	43.5
D: $(\bar{R}^{obs}, N^{opt})$	388	1315	64.7	94.4	29.7

Notes: Each panel corresponds to cost levels in the indicated year. $(\bar{R}^{opt}, N^{opt})$ denotes the welfare-maximizing pair, $(\bar{R}^{obs}, N^{obs})$ fixes both at observed levels in each year, and mixed cases optimize only one dimension while holding the other fixed at observed. The WTP and cost estimates are relative to that of an EV with a full range of 200km but without access to fast charging stations. Welfare= WTP-social cost.

Online Appendix

A Appendix A. Derivation of Bellman Equation (10)

We begin by discretizing time into intervals of length Δt. Within each interval, four events may occur:

1. Flow utility: The agent receives instantaneous flow utility $u(s)\,\Delta t$ from remaining in state s during the interval.

2. Travel transition: With probability $q_{s,s'}\Delta t$, the state transitions to $s' \neq s$ due to a travel event. Upon such a transition, the agent chooses between traveling ($j = 1$) and not traveling ($j = 0$), which yields the choice-specific values

$$\psi(1, s, s') + V(s') + \varepsilon_{t,1} \quad \text{or} \quad V(s) + \varepsilon_{t,0}.$$

3. Charging opportunity: With probability $\lambda_c \Delta t$, a charging opportunity arises. The agent then chooses whether to charge ($j = 1$) or not ($j = 0$), yielding the values

$$-c(1, s) + V(\bar{s}) + \varepsilon_{c,1} \quad \text{or} \quad V(s) + \varepsilon_{c,0}.$$

4. No event: With the remaining probability $1 - \sum_{s'} q_{s,s'}\Delta t - \lambda_c \Delta t$, no travel or charging event occurs, and the state remains s.

Because the model includes discounting at a rate ρ, each continuation value is divided by $(1 + \rho\Delta t)$. Putting these components together gives:

$$\begin{aligned} V(s) = u(s)\,\Delta t &+ \sum_{s'} \frac{q_{s,s'}\Delta t}{1 + \rho\Delta t} E \max_{j\in\{0,1\}} \Big\{\psi(1, s, s') + V(s') + \varepsilon_{t,1},\, V(s) + \varepsilon_{t,0}\Big\} \\ &+ \frac{\lambda_c \Delta t}{1 + \rho\Delta t} E \max_{j\in\{0,1\}} \Big\{ - c(1, s) + V(\bar{s}) + \varepsilon_{c,1},\, V(s) + \varepsilon_{c,0}\Big\} \\ &+ \frac{1 - \sum_{s'} q_{s,s'}\Delta t - \lambda_c \Delta t}{1 + \rho\Delta t} V(s). \end{aligned}$$

This recursion is a discrete-time approximation to the continuous-time Hamilton–Jacobi–Bellman (HJB) equation, which becomes exact as $\Delta t \to 0$ following the two steps below:

Step 1. Simplifying the expectation terms With i.i.d. Type I extreme value shocks, the

expectation of the maximum is:

$$E \max_{j\in\{0,1\}} \{v_j + \varepsilon_j\} = \sigma \ln \left(\sum_j e^{v_j/\sigma} \right) + \gamma\sigma,$$

where γ is the Euler–Mascheroni constant. Normalizing $\sigma = 1$ gives:

$$E \max\{\psi(1,s,s') + V(s'),\, V(s)\} = \ln\Big(e^{\psi(1,s,s')+V(s')} + e^{V(s)}\Big) + \gamma,$$
$$E \max\{-c(1,s) + V(\bar{s}),\, V(s)\} = \ln\big(e^{-c(1,s)+V(\bar{s})} + e^{V(s)}\big) + \gamma.$$

Substituting the log-sum expressions into the recursion, we obtain

$$\begin{aligned} V(s) = u(s)\,\Delta t &+ \sum_{s'} \frac{q_{s,s'}\Delta t}{1+\rho\Delta t} \Big\{ \ln\big(e^{\psi(1,s,s')+V(s')} + e^{V(s)}\big) + \gamma \Big\} \\ &+ \frac{\lambda_c \Delta t}{1+\rho\Delta t} \big\{ \ln\big(e^{-c(1,s)+V(\bar{s})} + e^{V(s)}\big) + \gamma \big\} \\ &+ \frac{1}{1+\rho\Delta t} \Big[1 - \sum_{s'} q_{s,s'}\Delta t - \lambda_c \Delta t \Big] V(s). \end{aligned}$$

Notice that the last term comes from the probability of staying in the same state when neither a travel nor a charging event occurs. At this stage, every coefficient is scaled by Δt and discounted by $1 + \rho\Delta t$.

Step 2. Taking the $\Delta t \to 0$ limit. To simplify, multiply both sides by $(1 + \rho\Delta t)$:

$$\begin{aligned} (1+\rho\Delta t)V(s) = u(s)\,\Delta t &+ \sum_{s'} q_{s,s'}\Delta t \Big\{ \ln\big(e^{\psi(1,s,s')+V(s')} + e^{V(s)}\big) + \gamma \Big\} \\ &+ \lambda_c \Delta t \Big\{ \ln\big(e^{-c(1,s)+V(\bar{s})} + e^{V(s)}\big) + \gamma \Big\} \\ &+ \Big[1 - \sum_{s'} q_{s,s'}\Delta t - \lambda_c \Delta t \Big] V(s). \end{aligned}$$

Bring the last term on the right-hand side together with the left-hand side:

$$\begin{aligned} (1+\rho\Delta t)V(s) - \Big[1 - \sum_{s'} q_{s,s'}\Delta t - \lambda_c \Delta t \Big] V(s) = u(s)\,\Delta t \\ + \sum_{s'} q_{s,s'}\Delta t \Big\{ \ln\big(e^{\psi(1,s,s')+V(s')} + e^{V(s)}\big) + \gamma \Big\} \\ + \lambda_c \Delta t \Big\{ \ln\big(e^{-c(1,s)+V(\bar{s})} + e^{V(s)}\big) + \gamma \Big\}. \end{aligned}$$

Simplify the coefficient on $V(s)$:

$$\big[(1+\rho\Delta t)-(1-\sum_{s'} q_{s,s'}\Delta t-\lambda_c\Delta t)\big]V(s)=(\rho+\lambda_c+\sum_{s'} q_{s,s'})\Delta t\, V(s).$$

Dividing both sides by Δt and taking the limit as $\Delta t \to 0$, we obtain:

$$\begin{aligned}(\rho+\lambda_c+\sum_{s'} q_{s,s'})V(s)=u(s)+\sum_{s'} q_{s,s'}\Big\{\ln\big(e^{\psi(1,s,s')+V(s')}+e^{V(s)}\big)+\gamma\Big\}\\ +\lambda_c\Big\{\ln\big(e^{-c(1,s)+V(\bar{s})}+e^{V(s)}\big)+\gamma\Big\}.\end{aligned}$$

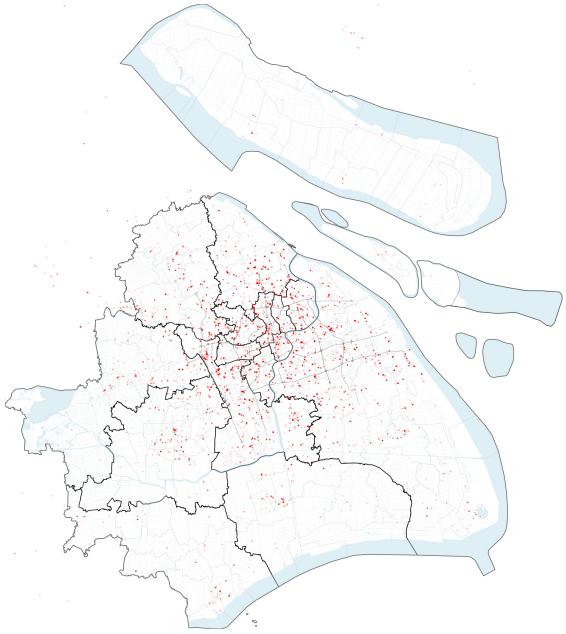
Dividing both sides gives (note we assume $u(s)=0$):

$$\begin{aligned}V(s)=&\frac{\sum_{s'} q_{s,s'}\Big\{\ln\big(e^{\psi(1,s,s')+V(s')}+e^{V(s)}\big)+\gamma\Big\}}{\rho+\lambda_c+\sum_{s'} q_{s,s'}}\\ &+\frac{\lambda_c\Big\{\ln\big(e^{-c(1,s)+V(\bar{s})}+e^{V(s)}\big)+\gamma\Big\}}{\rho+\lambda_c+\sum_{s'} q_{s,s'}},\end{aligned}$$

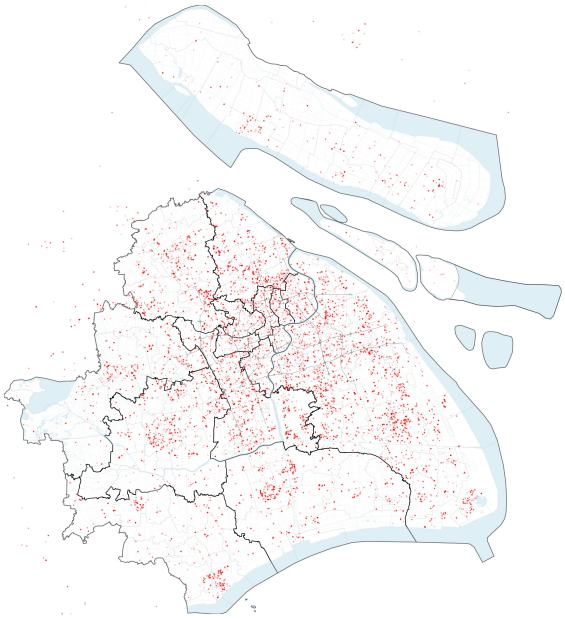
which matches Equation (10).

B Appendix Figures

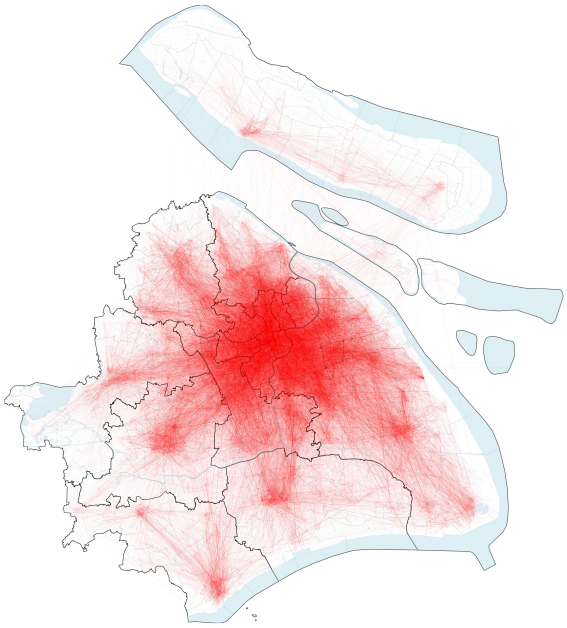
Figure A1: Descriptions of the EV Trip dataset



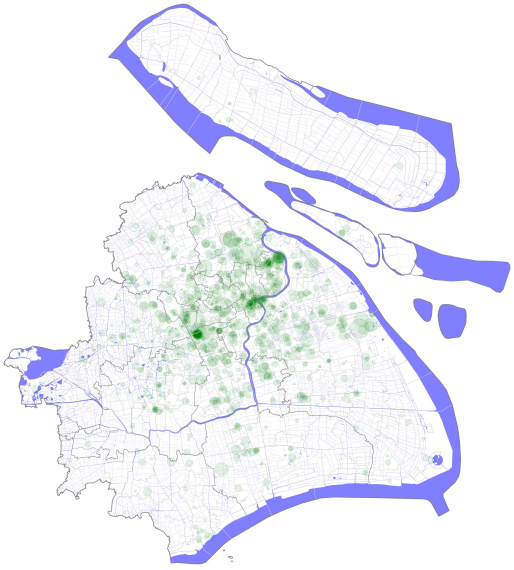
(a) Fast Charging Locations



(b) Slow Charging Locations



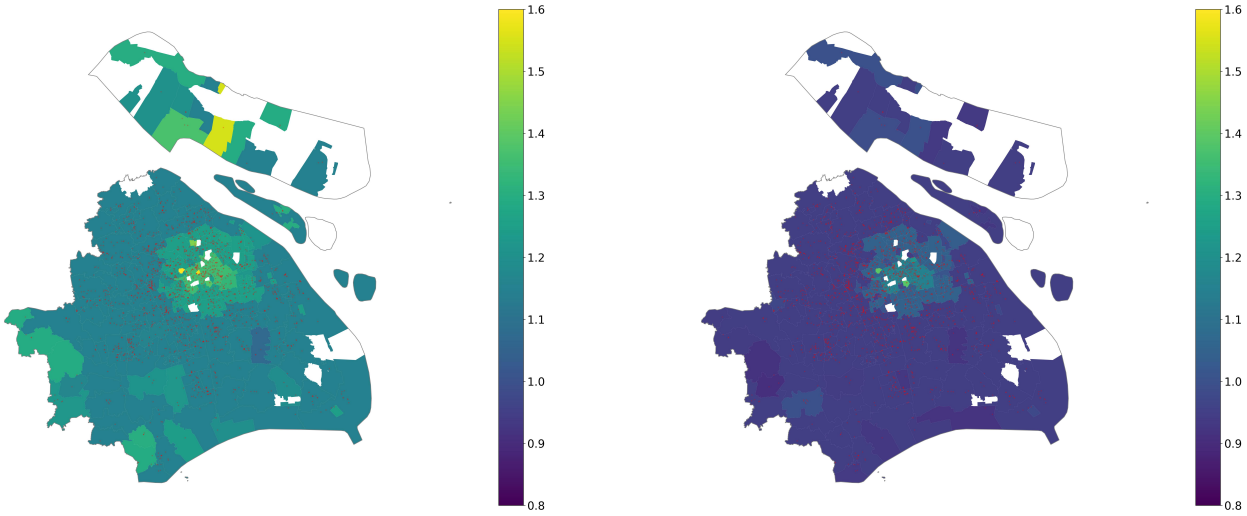
(c) Trip: Origin to Destination



(d) Fast Stations (weighted by usage)

Note: Figures (a)-(c) are constructed based on the eight-week EV charging sample. Figure (a) plots locations of the observed 8,524 fast charging; Figure (b) plots the locations of the 16,986 observed slow charging; Figure (c) plots the connected lines of 188,707 trip origins to destinations (excluding trips outside Shanghai for visualization). Figure (d) plots the fast charging station usages in 2024 from the charging network dataset sourced from Shanghai Electric Technology Center, and it aligns well with Figure (a), verifying the representativeness of the trip sample.

Figure A2: Charging Prices (¥/kWh) Cross Locations by Time

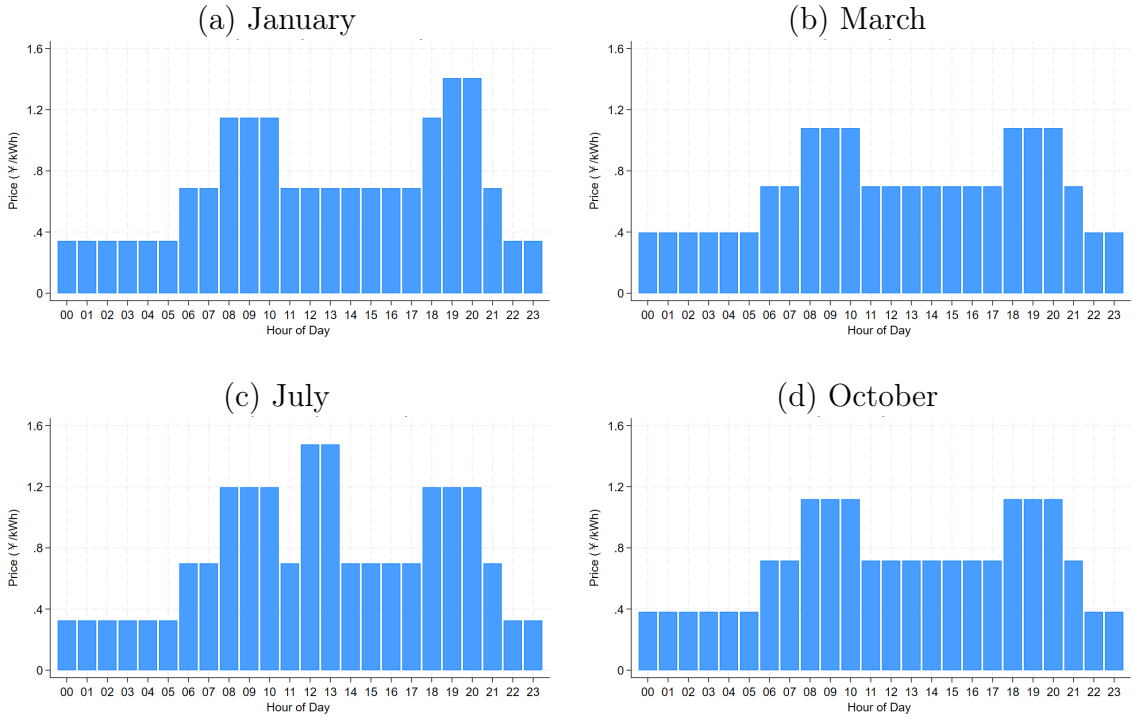


(a) Charging Price (noon)

(b) Charging Price (10 pm)

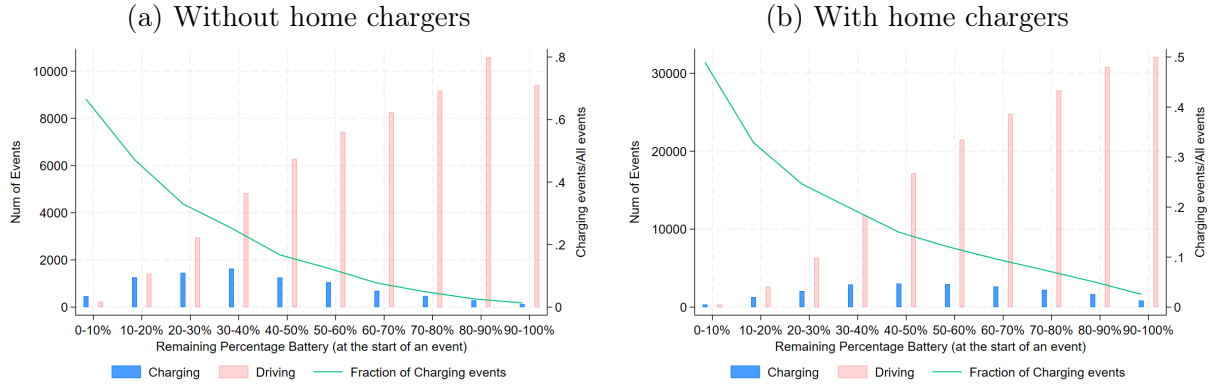
Notes: The plots show the average charging price (¥/kWh) in fast charging stations across locations in Shanghai around noon in Panel (a) and at 10pm in Panel (b) in our sample. Prices vary significantly across location, and are much higher around noon than at 10pm.

Figure A3: Electricity Prices by Month in 2024



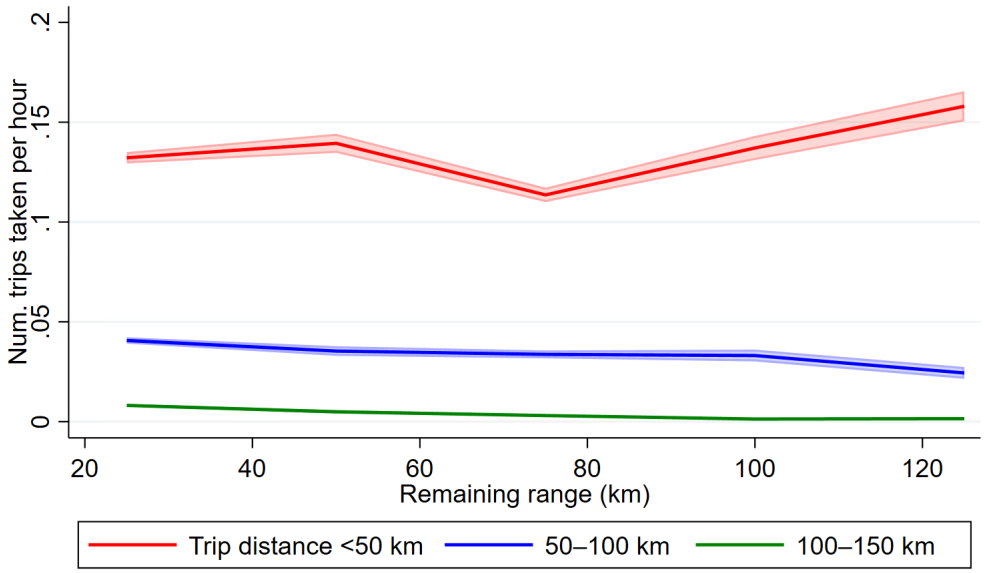
Notes: The plots depict hourly electricity prices (¥/kWh) in each of the four months in 2024 for home charging.

Figure A4: Number of Events by Remaining Battery: by home charger ownership



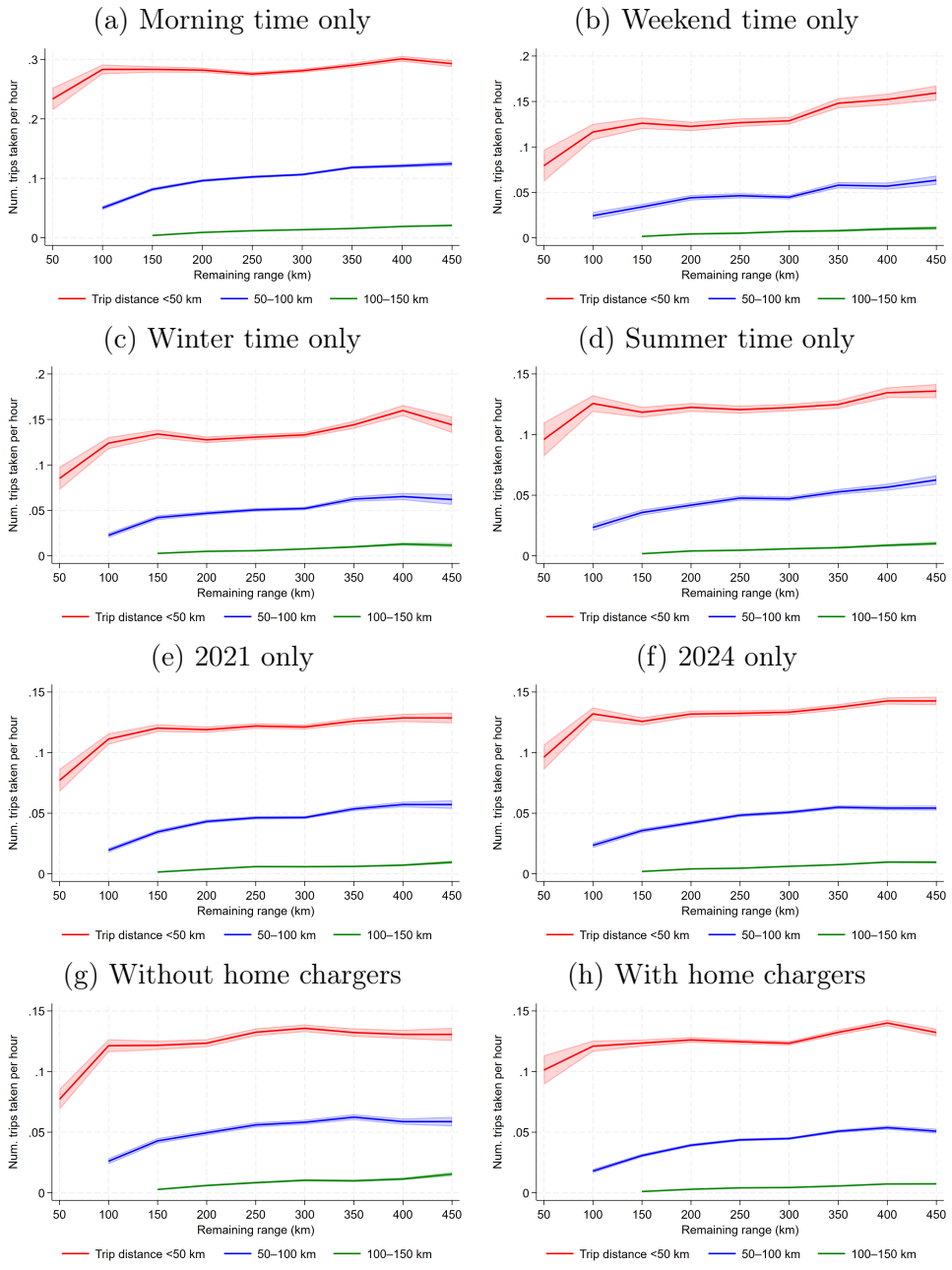
Notes: Each colored line corresponds to a trip with a certain distance: $<$ 50 km, 50–100 km, 100–150 km, and 150–200 km. Hazard rates by the y-axis are computed as the number of trips initiated per hour from each starting remaining range (x-axis), normalized by the hours vehicles stay in that state (until a trip arrives). Shaded areas show 95% confidence intervals. Each panel presents the results for a specific time frame. The overall pattern is consistent with that from pooling all the data together.

Figure A5: Placebo: No Missing Trips at Low SOC for PHEVs



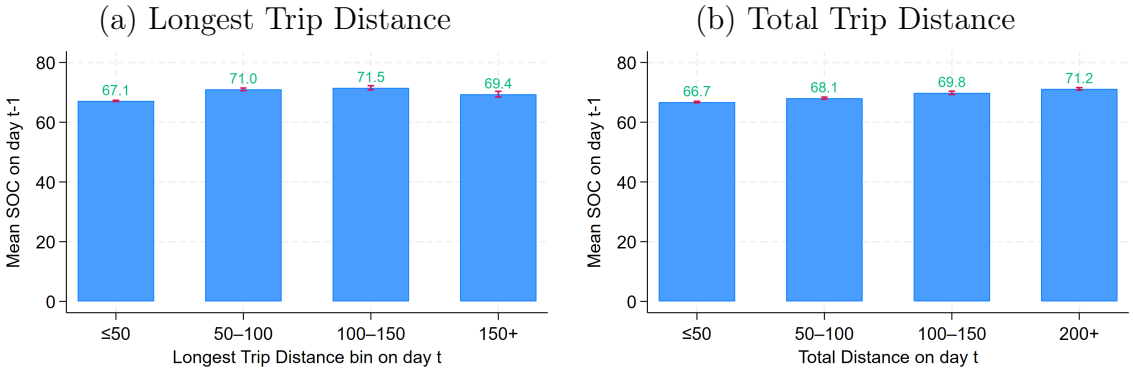
Notes: The data is based on the tracking data for 250 PHEVs in each of the 8 weeks as in the main sample for BEVs. Each colored line corresponds to a trip with a certain distance: $<$ 50 km, 50–100 km, 100–150 km, and 150–200 km. Hazard rates by the y-axis are computed as the number of trips initiated per hour from each starting remaining range (x-axis), normalized by the hours vehicles stay in that state (until a trip arrives). Shaded areas show 95% confidence intervals. Each panel presents the results for a specific time frame. The overall pattern is consistent with that from pooling all the data together.

Figure A6: Unrealized Trips at Low SOC



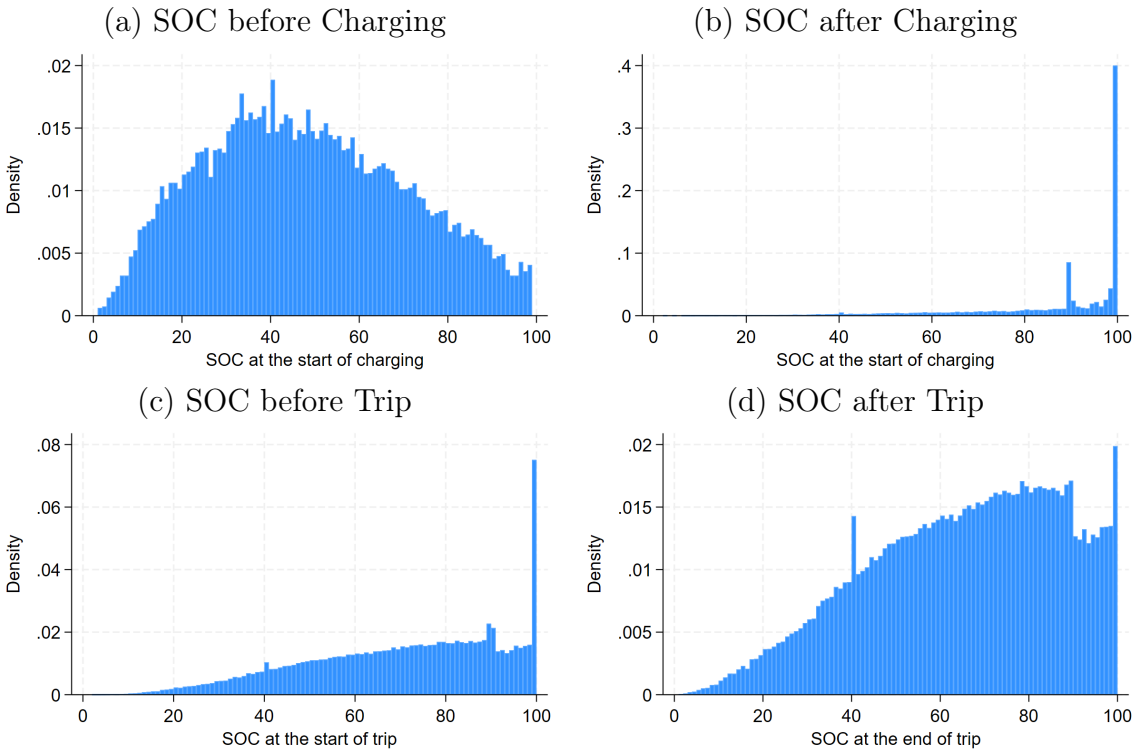
Notes: Each colored line corresponds to a trip with a certain distance: < 50 km, 50–100 km, 100–150 km, and 150–200 km. Hazard rates by the y-axis are computed as the number of trips initiated per hour from each starting remaining range (x-axis), normalized by the hours vehicles stay in that state (until a trip arrives). Shaded areas show 95% confidence intervals. Each panel presents the results for a specific time frame. The overall pattern is consistent with that from pooling all the data together.

Figure A7: Anticipation Charging: SOC Level at Day $t-1$ and Trip at day t



Notes: This figure presents the average SOC at day $t-1$, conditional on the trips taken at day t with Panel (a) showing the longest trip distance and Panel (b) showing the total trip distance in four bins: [0,50), [50,100), [100,150), [150, ∞). The SOC level seems flat and does not exhibit a strong correlation.

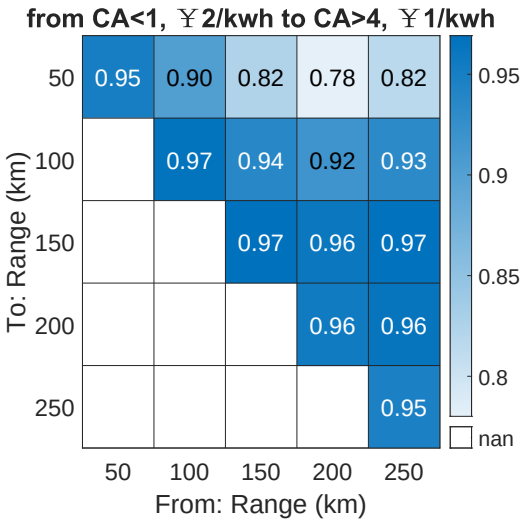
Figure A8: SOC Levels at Event Start and End



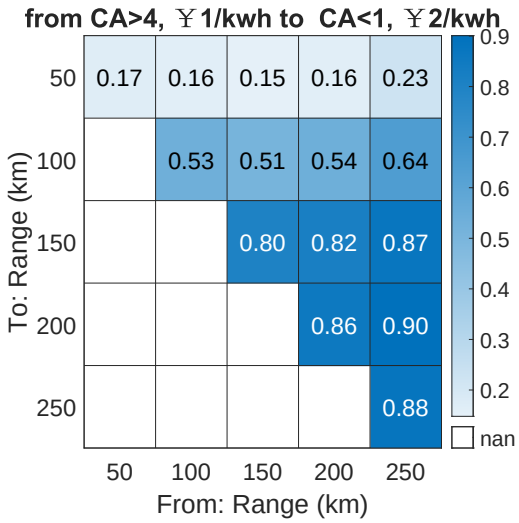
Notes: Panels (a) to (d) plot the distribution of observed events (charging or driving) with the starting or ending SOC at a given level. There is no evidence of systematic bunching at the 20% or 80% thresholds, suggesting that drivers do not adhere to the "20–80" heuristic for battery preservation.

Figure A9: Estimated Trip-taking Probability $h^{H=0,\bar{R}=500}(b, r, p)$

(a) Trip Probability



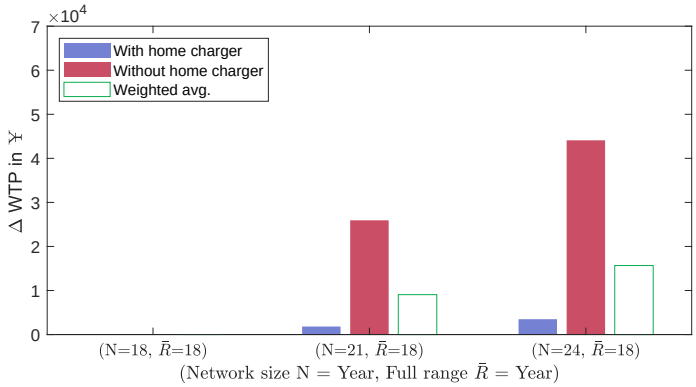
(b) Trip Probability



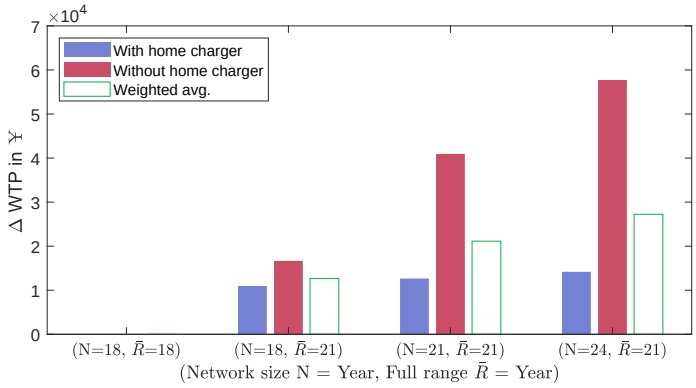
Notes: This figure presents the estimated policy functions governing charging and traveling decisions. Panels (a) and (b) display the probability of taking a trip with a starting range (x-axis) to an end range (y-axis). "Nan" denotes infeasible trips. Darker shades represent higher probabilities. Each heatmap cell corresponds to the probability of taking the trip that moves the car from a given initial range (x-axis) to a new remaining range (y-axis).

Figure A10: WTP Decomposition for EV Purchased in Different Years

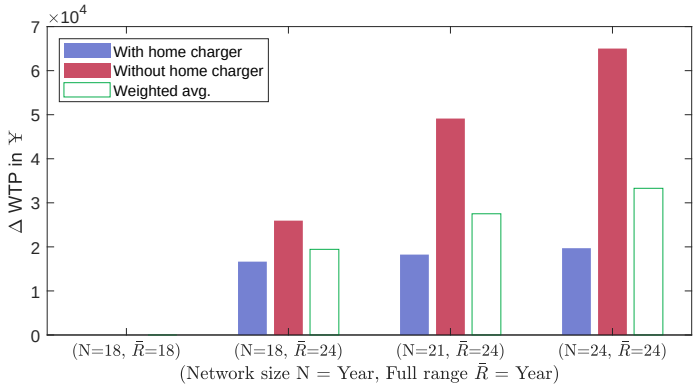
(a) An average EV bought in 2018



(b) An average EV bought in 2021



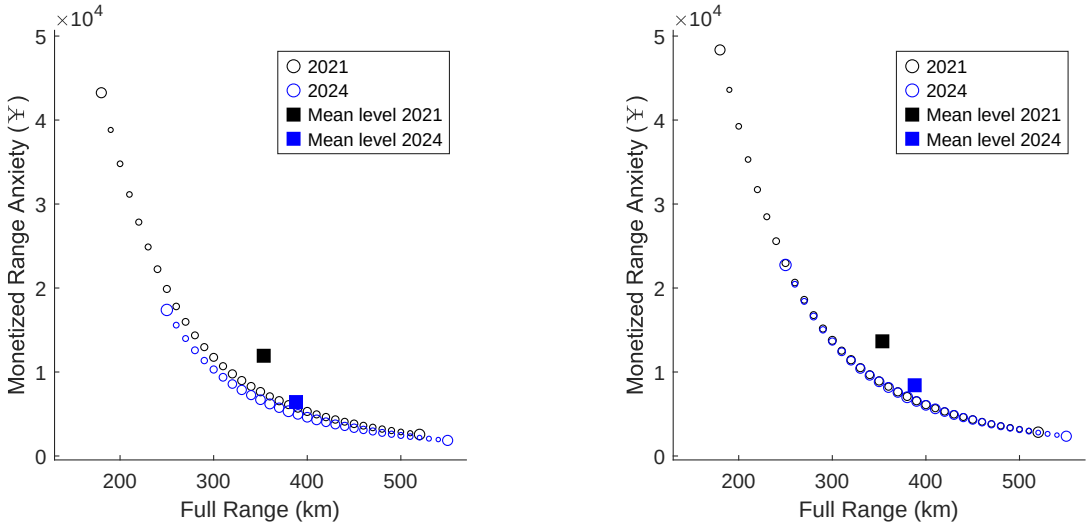
(c) An average EV bought in 2024



Notes: The plots depict the WTP for the expansion of charging network (from 2018 to 2021 or 2024 levels) and the improvement in driving range (from 2018 to 2021 or 2024 levels) separately for drivers with access to home charging and those without.

Figure A11: Range Anxiety by Access to Home Charging

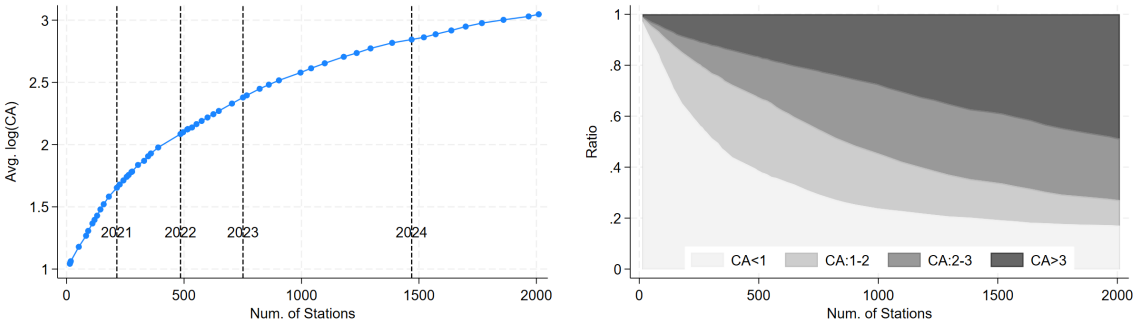
(a) Range anxiety w/o home chargers (b) Range anxiety with home chargers



Notes: Each panel plots *monetized range anxiety* (lifetime WTP, 10^4 ¥) against the vehicle's full range (km). Circle area is proportional to the empirical frequency of each full-range level in that year's sample. Filled squares mark the weighted mean level for the year. Panel (a) evaluates consumers *without* home charging; panel (b) evaluates consumers *with* home charging. The downward slope indicates that range anxiety declines with battery range; the downward shift from 2021 to 2024 reflects improvements in network size and prices.

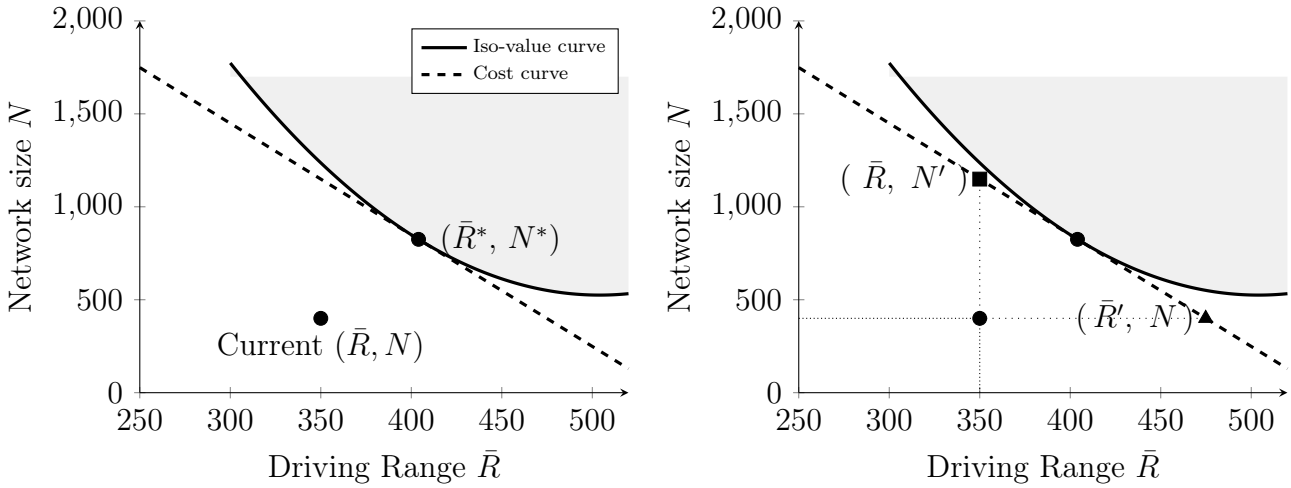
Figure A12: Relationship between Charging Access and the Number of Stations

(a) Average CA (b) $\Pr(CA = 1, 2, 3, 4)$



Notes: Charging access (CA) is an inverse–distance–squared index for each location i, $\text{CA}_i = \sum_j 1/\text{dist}_{ij}^2$, where nearby stations receive more weight. Panel (a) plots the sample average of log(CA) as the total number of stations increases; the vertical dashed lines mark the observed station counts in 2021–2024. The concavity indicates diminishing marginal improvements in access as the network grows. Panel (b) shows how the cross-sectional distribution of access shifts with network size: stacked areas are the shares of locations falling in four CA bins (< 1, 1–2, 2–3, > 3).

Figure A13: Policy Coordination between Driving Range and Network Size Investments



(a) Iso-value (solid) and cost (dashed) curves

(b) Single-technology strategy

Notes: The figure illustrates the role of policy coordination between investing in driving range R and investing in charging network size N. The solid curve is an iso-value (welfare) contour: combinations above the curve (light shading) deliver higher welfare. The dashed line is the budget line, representing relative prices that keep total cost constant along the line. Panel (a) shows the optimum at the tangency between the iso-value and cost curves $(\bar{R}^*, N^*)$; the current configuration $(\bar{R}, N)$ lies below. Panel (b) depicts the single-investment trajectory from the current point: moving vertically to $(\bar{R}, N')$ improves only network size, while moving horizontally to $(\bar{R}', N)$ improves only battery capacity, both along the same cost line. Because investment in $\bar{R}$ and N exhibits diminishing marginal returns, coordinated investments that move $(\bar{R}, N)$ toward the tangency achieves larger welfare gains than strategies that adjust only $\bar{R}$ or only N.

C Appendix Tables

Table A1: Dataset Overview

Year	2021				2024			
	Winter	Spring	Summer	Fall	Winter	Spring	Summer	Fall
Driver info								
# Drivers	1100	1100	1100	1100	1100	1100	1100	1100
Avg. range (km)	293	357	356	381	332	411	378	416
With home charger	75.1%	61.9%	62.8%	57.2%	67.0%	64.8%	66.7%	63.5%
Driving Trips per driver per week								
Count	20.9	20.3	20.5	20.9	23.4	21.6	21.7	21.7
Total distance (km)	376.4	388.5	381.8	405.6	477.2	447.1	447.6	514
Total duration (hour)	15.6	16.3	15.8	16.1	19.2	18.4	18.8	19
Chargings per driver per week								
# Fast	0.7	0.9	0.9	1.1	1.5	1.2	1.3	1.1
# Slow	2.5	1.9	1.9	1.6	3.5	2.4	2.6	2.1
Fast Duration (hour)	2.3	1.6	1.7	1.9	2.1	1.8	1.8	1.7
Slow Duration (hour)	14.7	13	13.3	11.7	13.6	11	12.4	12.2
Fast Starting SOC	35	37	34	33	40	44	39	39
Slow Starting SOC	47	48	45	45	49	50	46	45

Note: The dataset in each year includes four weekly cross-sections of 1100 randomly selected EVs from the EV stock in Shanghai during Jan 23-30 (Winter), March 20-27 (Spring), Aug 23-30 (Summer), and Oct 20-27 (Fall). In total, there are 188,707 driving trips, about 16,986 slow charging sessions, and about 8,524 fast charging sessions. Driving range is calculated based on the data: $\frac{\text{Total distance driven}}{\text{Total battery consumed}} \times \text{Battery Size}$.

Table A2: Empirical Evidence of Range Anxiety

	(1) Baseline	(2) Peak	(3) Weekend	(4) Winter	(5) Summer
$\mathbb{1}$(Range after a trip $<$ 50km)	-0.840***	-1.158***	-0.813***	-0.783***	-0.730***
	(0.0302)	(0.0625)	(0.0770)	(0.0552)	(0.0579)
$\mathbb{1}$(Range after a trip $\in$ 50–100km)	-0.140***	-0.321***	-0.178***	-0.0852***	-0.0746***
	(0.0175)	(0.0288)	(0.0400)	(0.0319)	(0.0287)
Jiedao FE	Yes	Yes	Yes	Yes	Yes
Trip distance bin $\times$ Year FE	Yes	Yes	Yes	Yes	Yes

Note: This table shows the PPML regression results from a Poisson model on the hazard rate of trips. The number of observations is 15,272 by *jiedao* (225) by year (2) by trip-bins (35). Jiedao is a sub-district administrative unit in Shanghai comparable to a census tract. For Columns (2)-(5), we limit the sample to peak-hour trips (weekday 6-9 am and 4-7 pm), weekend trips, trips in the winter (January), and trips in the summer (August). The jiedao FEs, and the trip distance bin by year FEs are included.

Table A3: Trip-Level Regression Using Speed as Instruments

Panel A: 1st Stage	Dep. var.: Range after a trip	
	(1) OLS	(2) OLS
Standardized residualized speed	0.918***	0.814***
	(0.052)	(0.038)
Start range	1.011***	1.011***
	(0.000)	(0.000)
Distance	-1.027***	-1.027***
	(0.003)	(0.003)
Distance × residualized speed		0.006**
		(0.002)
Driver FE	Yes	Yes
Hour-of-the-day FE	Yes	Yes
Jiedao FE	Yes	Yes

Panel B: Poisson Regression	Dep. var.: Hazard rate		
	(1) PPML	(2) IV-CF	(3) IV-CF
$\mathbb{1}$(Range after a trip $<$ 50 km)	-0.783***	-1.017*	-0.988*
	(0.037)	(0.523)	(0.507)
$\mathbb{1}$(Range after a trip$\in$ 50–100km)	-0.120***	-0.307***	-0.306***
	(0.018)	(0.102)	(0.101)
Fixed Effects: Trip Distance	Yes	Yes	Yes

Notes: This table reports results using residualized speed from the previous trip as an instrument for the remaining range after the next trip. Residualized $\widetilde{\text{Speed}}_{jt}$ is obtained from the trip-level regression on speed (calculated as distance over trip duration):

$$\text{Speed}_{jt} = \text{Origin-Destination-district FE}_j + \text{Hour-of-day FE}_t + \widetilde{\text{Speed}}_{jt}.$$

Panel A regresses the remaining range on start range, trip distance, and residualized speed. The number of observation is 170,642. Conditional on a trip characteristics, higher speed leads to higher remaining ranges, effectively providing a strong first stage that residualized speed can reflect traffic conditions and shift remaining ranges after a trip. Panel B replicates regression (3) at the trip level. Column (1) shows similar results as regression at jiedao level. Columns (2) and (3) in Panel B report IV estimates under PPML using the control function approach. The instruments for remaining range are residualized speed and its interaction with the distance of the previous trip. Column (3) additionally includes the interaction of speed and the starting range. Standard errors are clustered at the driver level. Significance levels: *** $p < 0.01$, ** $p < 0.05$, * $p < 0.1$.

Table A4: Model Estimates: State Arrival & Transition

	W/out Home Charging		W/ Home Charging	
	Estimate	SE	Estimate	SE
Trip Arrival (per day): daytime				
<50km	3.7267	(0.0487)	4.5121	(0.0808)
50-100km	1.5608	(0.0237)	1.5808	(0.0298)
100-150km	0.2438	(0.0068)	0.1546	(0.0045)
150-200km	0.0958	(0.0040)	0.0368	(0.0019)
200-250km	0.0334	(0.0023)	0.0099	(0.0009)
250-300km	0.0155	(0.0018)	0.0034	(0.0006)
300-350km	0.0093	(0.0017)	0.0017	(0.0006)
350-400km	0.0032	(0.0013)	0.0010	(0.0006)
Trip Arrival (per day): nighttime				
<50km	1.4052	(0.0316)	0.8933	(0.0179)
50-100km	0.7494	(0.0193)	0.4199	(0.0095)
100-150km	0.1983	(0.0079)	0.0706	(0.0027)
150-200km	0.0916	(0.0051)	0.0280	(0.0016)
200-250km	0.0459	(0.0035)	0.0103	(0.0010)
250-300km	0.0251	(0.0029)	0.0041	(0.0007)
300-350km	0.0107	(0.0023)	0.0009	(0.0004)
350-400km	0.0058	(0.0022)	0.0003	(0.0004)
Peak Transition				
Pr(OffPeak->Peak)	0.3545	(0.0096)	0.2536	(0.0065)
Pr(Peak->OffPeak)	0.2771	(0.0085)	0.4270	(0.0102)
Location Transition (2021)				
Pr(->CA $\in [0,1]$)	0.4181	(0.0034)	0.5037	(0.0025)
Pr(->CA $\in [1,2]$)	0.3277	(0.0032)	0.3130	(0.0023)
Pr(->CA $\in [2,3]$)	0.1443	(0.0024)	0.1213	(0.0016)
Pr(->Price $\in [0,1.2]$)	0.2498	(0.0030)	0.1994	(0.0020)
Pr(->Price $\in [1.2,1.5]$)	0.1717	(0.0026)	0.1991	(0.0020)
Pr(->Price $\in [1.5,2]$)	0.2969	(0.0031)	0.3865	(0.0024)
Pr(->Amenity $\in [0,1]$)	0.2151	(0.0028)	0.2120	(0.0020)
Pr(->Amenity $\in [1,2]$)	0.2073	(0.0028)	0.2573	(0.0022)
Pr(->Amenity $\in [2,3]$)	0.2550	(0.0030)	0.2668	(0.0022)
Pr(->W/ Private Charger)	0.0000	(NaN)	0.1985	(0.0020)
Location Transition (2024)				
Pr(->CA $\in [0,1]$)	0.1719	(0.0024)	0.2256	(0.0019)
Pr(->CA $\in [1,2]$)	0.0984	(0.0019)	0.1741	(0.0017)
Pr(->CA $\in [2,3]$)	0.2555	(0.0028)	0.2770	(0.0020)
Pr(->Price $\in [0,1.2]$)	0.2887	(0.0029)	0.2027	(0.0018)
Pr(->Price $\in [1.2,1.5]$)	0.1849	(0.0025)	0.2276	(0.0019)
Pr(->Price $\in [1.5,2]$)	0.2700	(0.0028)	0.3670	(0.0021)
Pr(->Amenity $\in [0,1]$)	0.2251	(0.0027)	0.2667	(0.0020)
Pr(->Amenity $\in [1,2]$)	0.2302	(0.0027)	0.2826	(0.0020)
Pr(->Amenity $\in [2,3]$)	0.2683	(0.0028)	0.2392	(0.0019)
Pr(->W/ Private Charger)	0.0000	(NaN)	0.2108	(0.0018)

Notes: The sample includes 8,000 drivers with 214,000 sessions. The table reports estimated Poisson trip arrival rates and transition probabilities by types.

Table A5: Model Estimates: Robustness checks

	(1) 25km Interval		(2) Distance Types	
Parameter	Estimate	S.E.	Estimate	S.E.
Trip utility				
α_0 (baseline trip utility)	2.0218	0.0226	2.4916	0.0129
α_1 (marginal utility per 50 km)	1.0585	0.0170	0.8164	0.0152
α_2 (anxiety: 50–100 km remaining)			-0.7953	0.0200
α_3 (anxiety: 0–50 km remaining)			-1.8197	0.0358
α_2 (anxiety: 75–100 km remaining)	0.0604	0.0319		
α_3 (anxiety: 50–75 km remaining)	-0.4092	0.0405		
α_4 (anxiety: 25–50 km remaining)	-1.3303	0.0606		
α_5 (anxiety: 0–25 km remaining)	-2.8368	0.0957		
Charging cost: drivers w/out home chargers				
β_0 (base cost)	-2.8452	0.0294	-2.5157	0.0260
β_1 (sensitivity to charging access)	0.6858	0.0106	0.6980	0.0100
β_2 (sensitivity to charging price)	-1.5229	0.0181	-1.4498	0.0163
Charging cost: drivers w/ home chargers				
when using fast charger:				
β_0^h (base cost)	-4.3653	0.0273	-4.3371	0.0257
β_1^h (sensitivity to charging access)	0.0480	0.0133	0.0648	0.0131
β_2^h (sensitivity to charging price)	-0.6772	0.0172	-0.7378	0.0162
when using home charger:				
β_3^h (base cost)	-0.6205	0.0181	-0.2449	0.0176
β_4^h (sensitivity to charging access)	0.0414	0.0115	0.0000	0.0113
β_5^h (sensitivity to charging price)	-1.4086	0.0312	-1.6095	0.0304

Notes: The number of observations is 8,000 drivers with 214,000 sessions. Table reports the robustness checks on estimated structural parameters that govern the charging and driving choices: Consumers without home chargers: $C(\text{charging}, s) = \beta_0 + \beta_1(\text{CA}) + \beta_2(\text{price}) + \beta_3(\text{amenity})$. Consumers with home chargers: $C(\text{charging}, s) = \mathbb{1}(\text{not home}) \times (\beta_0^h + \beta_1^h(\text{CA}) + \beta_2^h(\text{price})) + \mathbb{1}(\text{home}) \times (\beta_3^h + \beta_4^h(\text{CA}) + \beta_5^h(\text{price}))$. Utility from trips: $\psi(\text{trips}, k, s) = \alpha_0 + \alpha_1(\text{trip distance}) + \alpha_2 \mathbb{1}(b_k \in [50, 100]) + \alpha_3 \mathbb{1}(b_k \in [0, 50]) + \alpha_4(\text{amenity})$, where b_k denotes remaining range after trip. The first specification (25 Km interval) further splits the remaining range into 25 km instead of 50 km bins. The second specification (Distance types) adds more granular types based on the average daily trip distance above or below the median. The estimates are close to the main specification in Table 3.